AD-A170 981 SUPERCONDUCTING CAVITY DEVELOPMENT FOR FREE ELECTRON LASERS(U) TRW ELECTRONICS AND DEFENSE SECTOR REDONDO BEACH CA MILITARY ELECTRONICS DIV G R NEIL ET AL. 1/1

UNCLASSIFIED 30 JUN 86 N00014-84-C-0667 F/G 20/5 NL

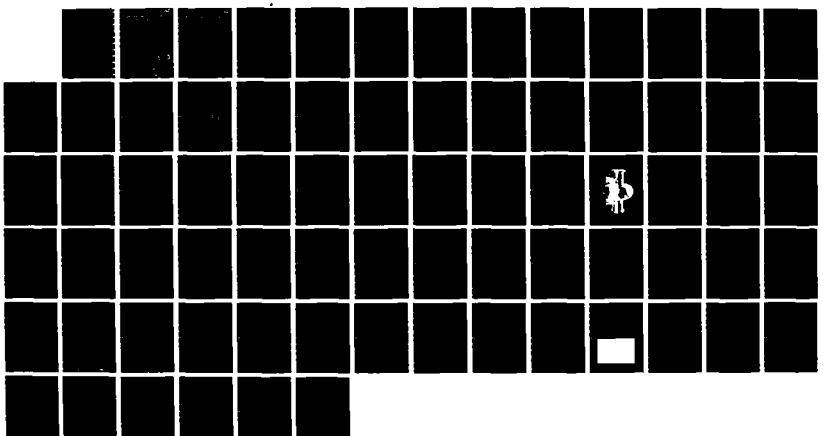

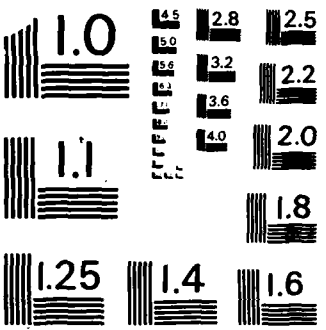

Contract N00014-84-C-0667

(12)

TRW

Superconducting Cavity Development for Free Electron Lasers

G.R. Neil, H.E. Boehmer, H.P. Demroff,
J.A. Edighoffer, S.W. Fornaca, J.L. Orthel,
M.A. Rhodes

Applied Technology Division
TRW Space & Technology Group
One Space Park, Redondo Beach, CA 90278

and
H.A. Schwettman, C.E. Hess, T.I. Smith, V. Nguyen-Tuong

Stanford University
High Energy Physics Laboratory

June 1986

Final Report for Superconducting Module Development Program

Office of Naval Research
1030 East Green Street
Pasadena, CA 91106

TRW

Superconducting Cavity Development for Free Electron Lasers

G.R. Neil, H.E. Boehmer, H.P. Demroff, J.A. Edighoffer, S.W. Fornaca, J.L. Orthel, M.A. Rhodes

Applied Technology Division
TRW Space & Technology Group
One Space Park, Redondo Beach, CA 90278

and

H.A. Schwettman, C.E. Hess, T.I. Smith, V. Nguyen-Tuong

Standord University
High Energy Physics Laboratory

June 1986

Final Report for Superconducting Module Development Program

Office of Naval Research
1030 East Green Street
Pasadena, CA 91106

Unclassified
SECURITY CLASSIFICATION OF THIS PAGE

AD-A170 981

REPORT DOCUMENTATION PAGE

1a. REPORT SECURITY CLASSIFICATION: Unclassified	1b. RESTRICTIVE MARKINGS
2a. SECURITY CLASSIFICATION AUTHORITY	3. DISTRIBUTION/AVAILABILITY OF REPORT
2b. DECLASSIFICATION/DOWNGRADING SCHEDULE	
4. PERFORMING ORGANIZATION REPORT NUMBER(S)	5. MONITORING ORGANIZATION REPORT NUMBER(S)
6a. NAME OF PERFORMING ORGANIZATION: TRW ELECTRONICS & DEFENSE APPLIED TECHNOLOGY DIVISION; 6b. OFFICE SYMBOL (If applicable): 01/1010	7a. NAME OF MONITORING ORGANIZATION
6c. ADDRESS (City, State and ZIP Code): One Space Park, Redondo Beach, CA 90278	7b. ADDRESS (City, State and ZIP Code)
8a. NAME OF FUNDING/SPONSORING ORGANIZATION: Office of Naval Research; 8b. OFFICE SYMBOL (If applicable): ONR	9. PROCUREMENT INSTRUMENT IDENTIFICATION NUMBER: N00014-84-C-0667
8c. ADDRESS (City, State and ZIP Code): 1030 E. Green Street, Pasadena, CA 91106	10. SOURCE OF FUNDING NOS. — PROGRAM ELEMENT NO. / PROJECT NO. / TASK NO. / WORK UNIT NO.
11. TITLE (Include Security Classification): Superconducting Cavity Development for Free Electron Lasers	
12. PERSONAL AUTHOR(S): G. Neil, H. Boehmer, H. Demroff, J. Edighoffer, S. Fornaca, J. Orthel, M. Rhodes, H. Schwettman, C. Hess, T. Smith and V. Nguyen-Tuong	
13a. TYPE OF REPORT: Final; 13b. TIME COVERED: FROM 7/84 TO 6/86	14. DATE OF REPORT (Yr., Mo., Day): 1986 June 30; 15. PAGE COUNT
16. SUPPLEMENTARY NOTATION	
17. COSATI CODES — FIELD / GROUP / SUB. GR.	18. SUBJECT TERMS (Continue on reverse if necessary and identify by block number): Free Electron Laser, Linear Accelerator, RF Superconductivity

19. ABSTRACT (Continue on reverse if necessary and identify by block number)

Significant progress was made toward the goal of developing cavity modules for a superconducting linear accelerator to drive a high average power Free Electron Laser. Through a combination of numerical modeling and experimental testing, a cavity geometry was developed that has the desired RF characteristics and that is ammenable to manufacture. Where possible, modifications to existing coupler designs were made to enhance their performance; weaknesses in coupler design were identified and addressed. A compact fully-integrated accelerator module, which could be replicated to form a high power FEL accelerator, was designed conceptually; features included cryostat, cavities, couplers and tuning mechanism. Facilities for fabricating full-size superconducting cavities meeting all technical requirements were initiated. Gradient enhancement tests on superconducting subscale models of the cavity were performed successfully.

20. DISTRIBUTION/AVAILABILITY OF ABSTRACT: UNCLASSIFIED/UNLIMITED ☒ SAME AS RPT. ☐ DTIC USERS ☐	21. ABSTRACT SECURITY CLASSIFICATION: UNCLASSIFIED
22a. NAME OF RESPONSIBLE INDIVIDUAL: George R. Neil	22b. TELEPHONE NUMBER (Include Area Code): (213) 535-2936; 22c. OFFICE SYMBOL: 01/1010

DD FORM 1473, 83 APR — EDITION OF 1 JAN 73 IS OBSOLETE.

UNCLASSIFIED
SECURITY CLASSIFICATION OF THIS PAGE

TABLE OF CONTENTS

FIGURE CAPTIONS

FIGURE 2-1: 500 MHz; (a) Initial CERN Design; (b) Optimum Design for High Power FEL Accelerator

FIGURE 2-2: Accelerator Mode Electric Field Profile

FIGURE 2-3: Cavity Distortion; (a) Underformed cavity total length is 70 cm; (b) Evacuated cavity maximum displacement from equilibrium is .3 mm; (c) Evacuated cavity with 750 lb. axial tension, maximum displacement from equilibrium is .13 mm.

FIGURE 2-4: HOM Electric Field Profiles; (a) Propagating mode, (b) Trapped mode above cut-off.

FIGURE 2-5: Frequency shifts of modes frequency shifts of first twelve symmetric monopole modes under cavity deformations shown in Figure 2-3.

FIGURE 2-6: Wakefield generation by a 30 ps bunch. The location and profile of the beam are shown below the dashed lines.

FIGURE 2-7: Wakepotential trailing a 60 ps. bunch.

FIGURE 2-8: Harmonic acceleration permits long bunches. Energy spread and emittance growth are minimized.

FIGURE 3-1: Selectivity based on symmetry properties aids mode identification and isolation.

FIGURE 3-2: Antisymmetric monopole modes in aluminum cavity.

FIGURE 3-3: Full scale copper model of cavity with coupler and diagnostic probes.

FIGURE 3-4: High power input coupler.

FIGURE 3-5: Higher order mode coupler with filter.

FIGURE 4-1: Beamline dewar.

TABLE CAPTIONS

1.0 INTRODUCTION

Research in Free Electron Lasers (FELs) has made considerable progress in the fourteen years since the first observation of radiation at Stanford University.[1] Experiments have progressed from the demonstration of oscillation with a constant wiggler system[2] through the measurement of gain and efficiency using a tapered wiggler oscillator system for efficiency enhancement.[3] As the FEL interaction is becoming better characterized, attention is shifting from physics demonstrations to real applications, with an eye to various high power strategic and tactical missions.

In making the transition from an FEL physics demonstration device to a useful high average power laser, one immediately sees an inadequecy in current technology. The linear accelerator (linac) necessary to drive the FEL must transport an average current that is orders of magnitude larger than is done today. Further, in addition to the average current required, the quality of the electron beam needed for the FEL interaction to take place imposes severe restrictions on the accelerator. In fact, even today's low average power linacs are only marginally suitable for FEL physics demonstrations; conventional technology has been stretched too close to its limits.

By examining the linac requirements from first principles, using an accelerator physics standpoint, one sees that in order to transport large currents usefully (for an FEL) the accelerator cavities should have certain characteristics. The cavities should have large apertures, high accelerating gradients and should operate cw rather than pulsed. The only practical way of combining these three features is to use superconducting cavities. Additionally, for maximum stability the cavities should be low frequency single-cell structures. The Superconducting Module Development Program is directed toward developing superconducting cavities and supporting devices (e.g. couplers, etc.) for a linac specifically intended to drive a high power FEL.

1.1 CAVITY REQUIREMENTS

Cavity and coupler requirements are soft, depending to a large extent on the configuration of the accelerator. For example, assuming that the linac requirements for a 10MW FEL might be as follows

Linac

E_{beam} = 100 MV
I_{ave} = 1 A
ϵ_N = .003 cm-rad
$\Delta E/E$ = .5%
Same cell energy recovery

the cavity gradient is determined by the number of cavities. The power coupling is determined by the optical power and the number of cavities. (If separate-cell energy recovery or no energy recovery were used, the electron beam power

would determine coupler requirements rather than optical power). Both of the following configurations are stable: (a) 50 cavities with 2 MV gain (6.7 MV/m) and 200kW coupling and (b) 33 cavities with 3 MV gain (10 MV/m) and 300 kW coupling. Both gradients are achievable. Both coupling levels are achievable, perhaps using only a single coupler and certainly by using two couplers. Which configuration to choose depends on considerations other than the linac design.

With this flexibility in mind, requirements for the superconducting cavity can be set somewhat arbitrarily.

Cavity

$E_{acc\ min} = 6.7$ MV/m
$f_o = 500$ MHz
$V_{min} = 2$ MV
$Q_o = 10^9$ (fundamental)
$Q_o = 10^4$ (other modes)

Coupling

$P_{coupler} = 150$ kW
$Q_{coupler} = 2.5 \times 10^5$ (critical coupling)

1.2 SUMMARY OF WORK PERFORMED

This program initiated an effort to determine the operational capabilities Of a superconducting cavity as optimized for utilization in a high average current electron linac intended as an FEL driver. During the program, the cavity configuration was established using computer modeling methods; its suitability for operation in a linac was determined. A full size copper model of the cavity, fitted

with input and higher order mode couplers, was bench tested. Facilities for the fabrication, processing, assembly and testing of a complete superconducting module were initiated. Gradient enhancement tests on subscale models were performed.

2. CAVITY MODELING AND ANALYSIS

The modeling activity supported the overall goal of designing a cavity system that could be used to drive a high current superconducting electron accelerator for FELs. This included not only designing and analyzing the cavity but optimizing the way the accelerator must be operated.

2.1 CAVITY DESIGN

The cavity was designed and the properties optimized for the fundamental (accelerator) mode. The mechanical and microwave properties were analyzed.

2.1.1 Shape Generation The cavity geometry was determined by starting with the CERN design[4] [see Figure 2.1 (a)] and modifying it to obtain additional features deemed desirable for the cavity. Using the code URMEL 2.0 the cavity was redesigned incorporating the following features. The shape of the cavity was modified until it reached the desired fundamental frequency. The final cavity geometry is shown in Figure 2.1(b). The modifications included an enlarged beam pipe (for improved HOM properties) and sloping walls (for improved chemical processing). The purpose of the circular cross-section is to reduce electron multipactoring near the cavity equator.

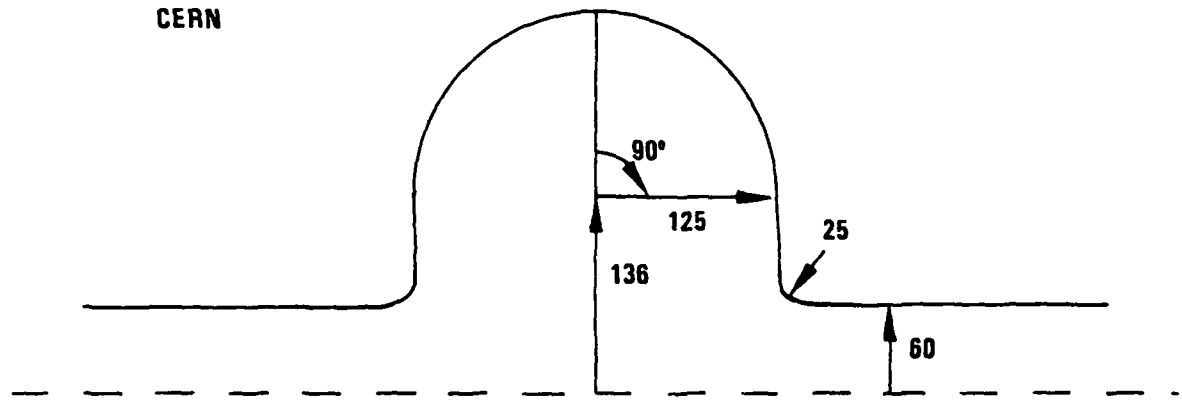

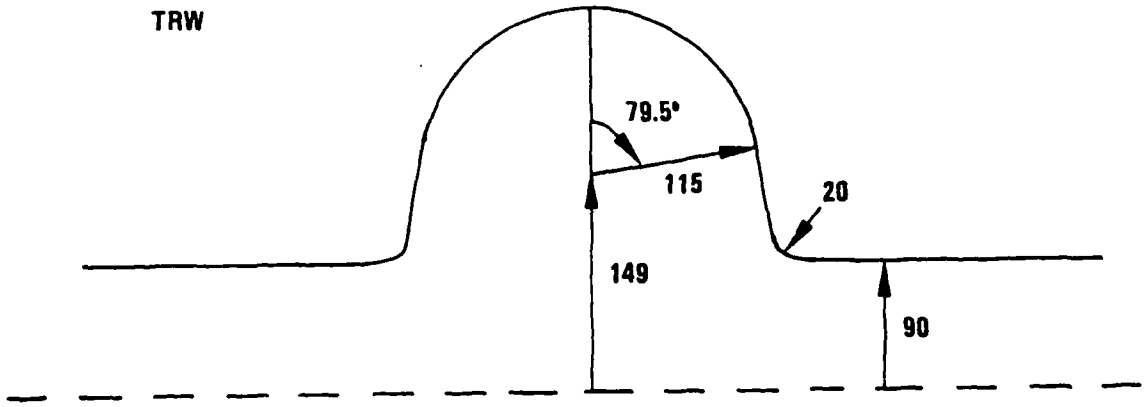

FIGURE 2-1: 500 MHz Cavity and Design
(a) Initial CERN Design
(b) Optimum Desing for High Power FEL Accelerator

The accelerator field configuration as computed by URMEL is shown in Fig 2.2. The mode parameters are summarized in Table 2.1. These include not only the fundamenatal parameters (frequency, normalized shunt impedance, etc.) but some operational parameters as well, based on the current level of technology. The power levels quoted are for copper; the power dissipation in a superconducting cavity is dependent on the processing history and operating temperature, but is typically five orders of magnitude lower.

2.1.2 Mechanical Properties An estimation of the response of the cavity to stress (such as tuning the cavity) was made using the nodal analysis program, NASTRAN. The force-free cavity geometry as input to NASTRAN is shown in Figure 2.3(a). It was assumed that the cavity was formed of high purity niobium sheet, 3 mm thick. Figure 2.3(b) is a grossly exaggerated view of the cavity distortion when it is evacuated and the outside remains at the 1 atmosphere; the maximum axial displacement occurs where the flat sides of the cavity bow inward. Crush strength of the cavity is twelve atmospheres. Figure 2-3(c) is a view of the evacuated cavity when subjected to 750 lb axial tension.

2.1.3 Tuning The frequency shifts caused by stress-induced geometry changes were calculated using the field values at the cavity boundary (from URMEL), the displacement

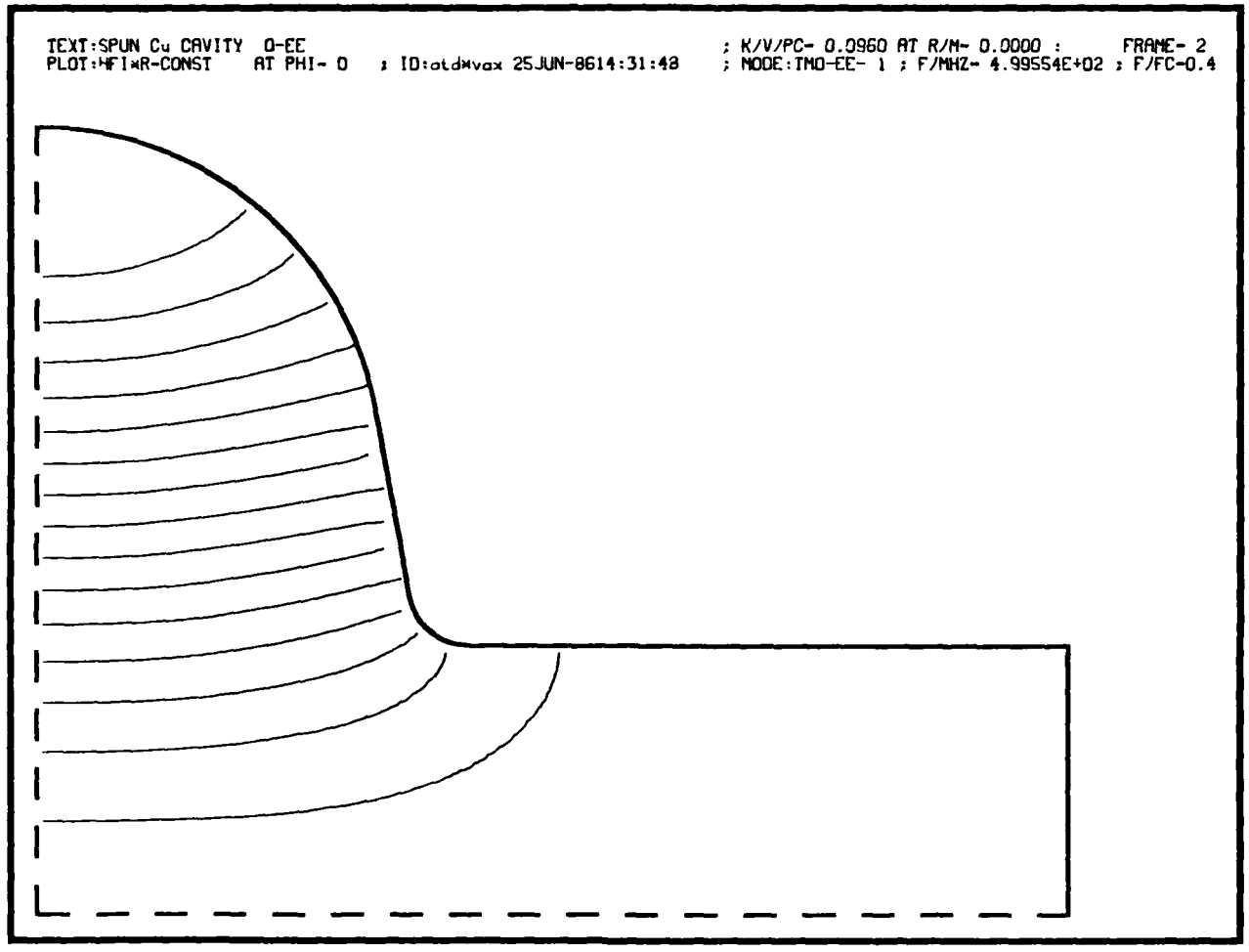

FIGURE 2-2: Accelerator Mode Electric Field Profile

FUNDAMENTAL MODE PARAMETERS

f_o = 499.6 MHz

λ_o = .600 m

f_c = 1275 MHz

R/Q = 122.4 ohm

Q_{Cu} = 44268

	URMEL OUTPUT	LOW GRADIENT	HIGH GRADIENT
V (MV)	2.07×10^{-3}	2.0	3.0
E_{acc} (MV/m)	6.91×10^{-3}	6.67	10.0
U_{store} (J)	1.12×10^{-5}	10.4	23.4
P_{wall} (MW)	7.94×10^{-7}	.74	1.66

TABLE 2-1

a) UNDEFORMED CAVITY TOTAL LENGTH IS 70 cm

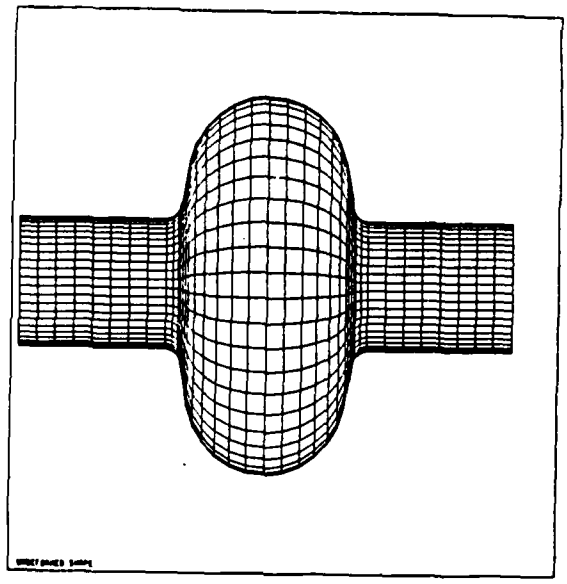

b) EVACUATED CAVITY MAXIMUM DISPLACEMENT FROM EQUILIBRIUM IS .3 mm

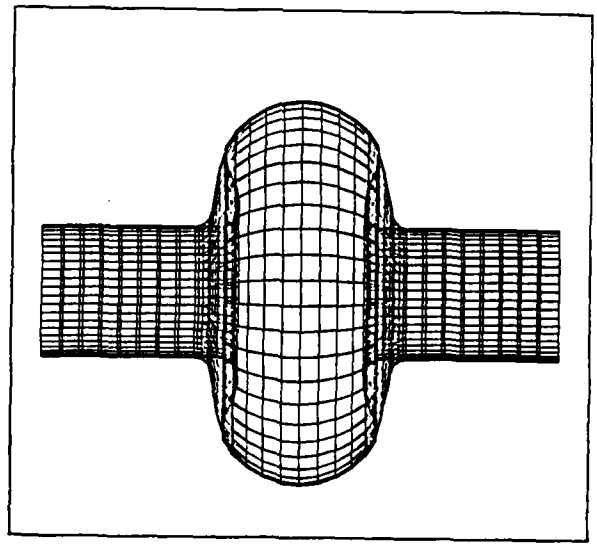

c) EVACUATED CAVITY WITH 750 lb. AXIAL TENSION

MAXIMUM DISPLACEMENT FROM EQUILIBRIUM IS .13 mm

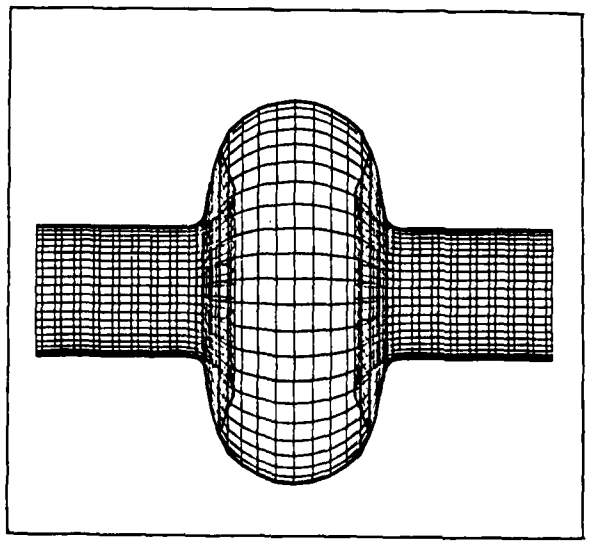

FIGURE 2-3: Cavity Distortion

of the boundary from equilibrium (from NASTRAN), and the Slater perturbation theorem. The result is the fundamental cavity resonance will shift 200 kHz in frequency as the cavity evacuates, but will approach its original value as the tension from the tuning mechanism increases.

2.2 HIGHER ORDER MODES (HOMS)

In addition to the fundamental mode, the cavity will support an infinite number of higher order modes. Most of these modes cannot couple to the beam, but some can. Monopole modes can cause add energy spread to the beam, making it unusable for the FEL; dipole modes can cause beam breakup instabilities. In addition to these (most dangerous) modes, at extremely high average currents quadrupole modes can be excited that would spoil the beam emittance. The monopole, dipole and quadrupole modes of supported by the cavity were analyzed.

2.2.1 Closed Cavity URMEL was used to predict the properties of the higher order modes supported by the closed cavity. All monopole, dipole and quadrupole modes up to 5 GHz (10 times the fundamental frequency) were calculated (with the exception of the TE_{0np}-like modes, which do not interact with a beam on axis). The modes were further classified as being either symmetric or antisymmetric (in z) about the cavity equator.

For the modes above the waveguide cut-off frequency of the beam pipe, the mode properties depend on the length of the cavity including the beam pipe and the boundary condition at the wall. To account for the fact that the boundary conditions in an accelerator are ambiguous (there is no metal wall between cavities) the actual frequencies are bracketed by assuming either an E-type boundary or an M-type boundary. (The latter is unphysical if the boundary is truly a conducting wall). The actual frequency will lie between these two extremes.

The field patterns for the modes were analyzed and field coupling strengths at symmetry points such as the equator and the end plates were calculated. This permitted an estimation of the signal strengths expected in the experimental measurements. Some sample field patterns as shown in Figure 2-4. In (a), a typical mode is shown; (b) shows a mode with little field extending into the beam pipe, and is therefore hard to excite or detect with an axial probe.

2.2.2 Open Cavity Trapped modes like that shown in Figure 2-4(b) are potentially very damaging. Unlike that of propagating modes, their power cannot be coupled easily from the cavity. This means that any coupling scheme must take these modes into account. To determine which modes might be

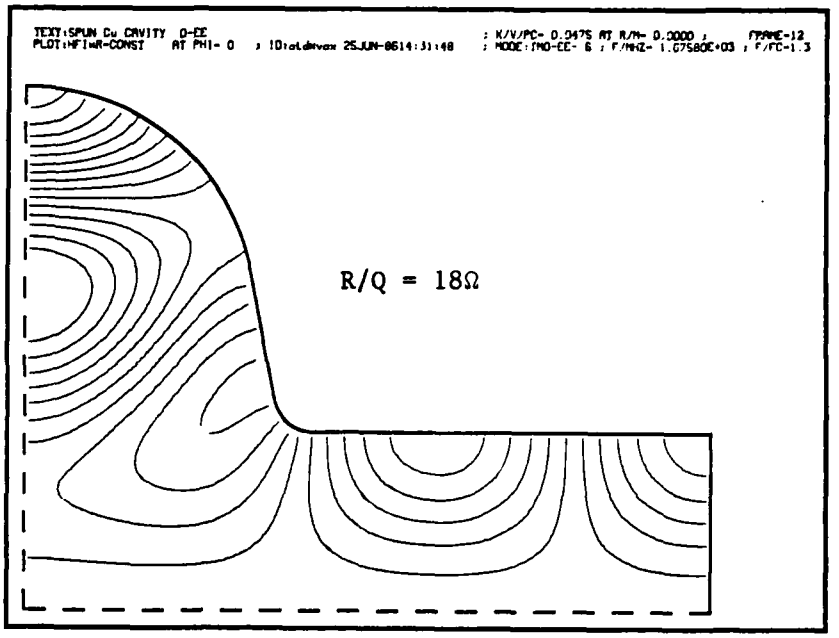

a) PROPAGATING MODE

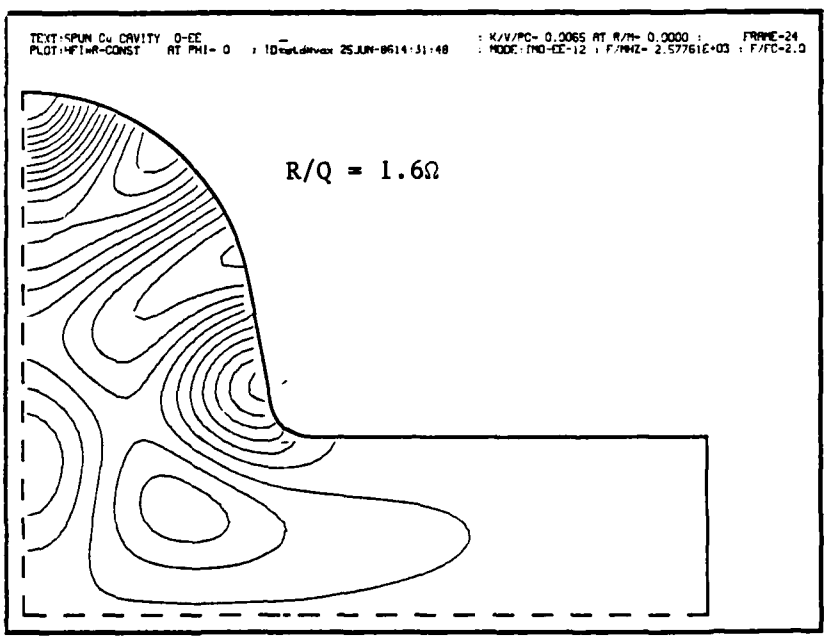

b) TRAPPED MODE ABOVE CUT-OFF

FIGURE 2-4: HOM Electric Field Profiles

troublesome, URMEL data was used to analyze an "open" cavity, that is, one whose reflecting endplates have been replaced with matched loads. The field pattern of each mode at the edge of the cavity was broken into the waveguide modes of the beam pipe. The power in the propagating waveguide modes (power that would not be reflected in the absence of a wall) was compared to the power dissipated in the cavity ohmically. In most cases, the power travelling down the beam pipe was much larger. In the case of the trapped modes, the propagating power is small in comparison.

The trapped cavity modes do not couple to propagating modes due to a mismatch in the radial structure of the fields at the cavity-beampipe interface. This analysis seems to hold for modes above and below the waveguide cutoff frequency of the beampipe. For example, the cavity might try to drive a n=3 radial mode into a circular waveguide that could only support an n=2 mode at that frequency. The phenomenon of some modes being trapped above cut-off seems to be universal. Of the geometries we have examined, all have exibited at least one trapped mode.

2.2.3 HOM Tuning Just as the fundamental mode shifts its frequency as the cavity is tuned, so do the higher order modes. Figure 2-5 is a plot of the mode shifts caused by cavity evacuation and by the addition of 750 lb tension for

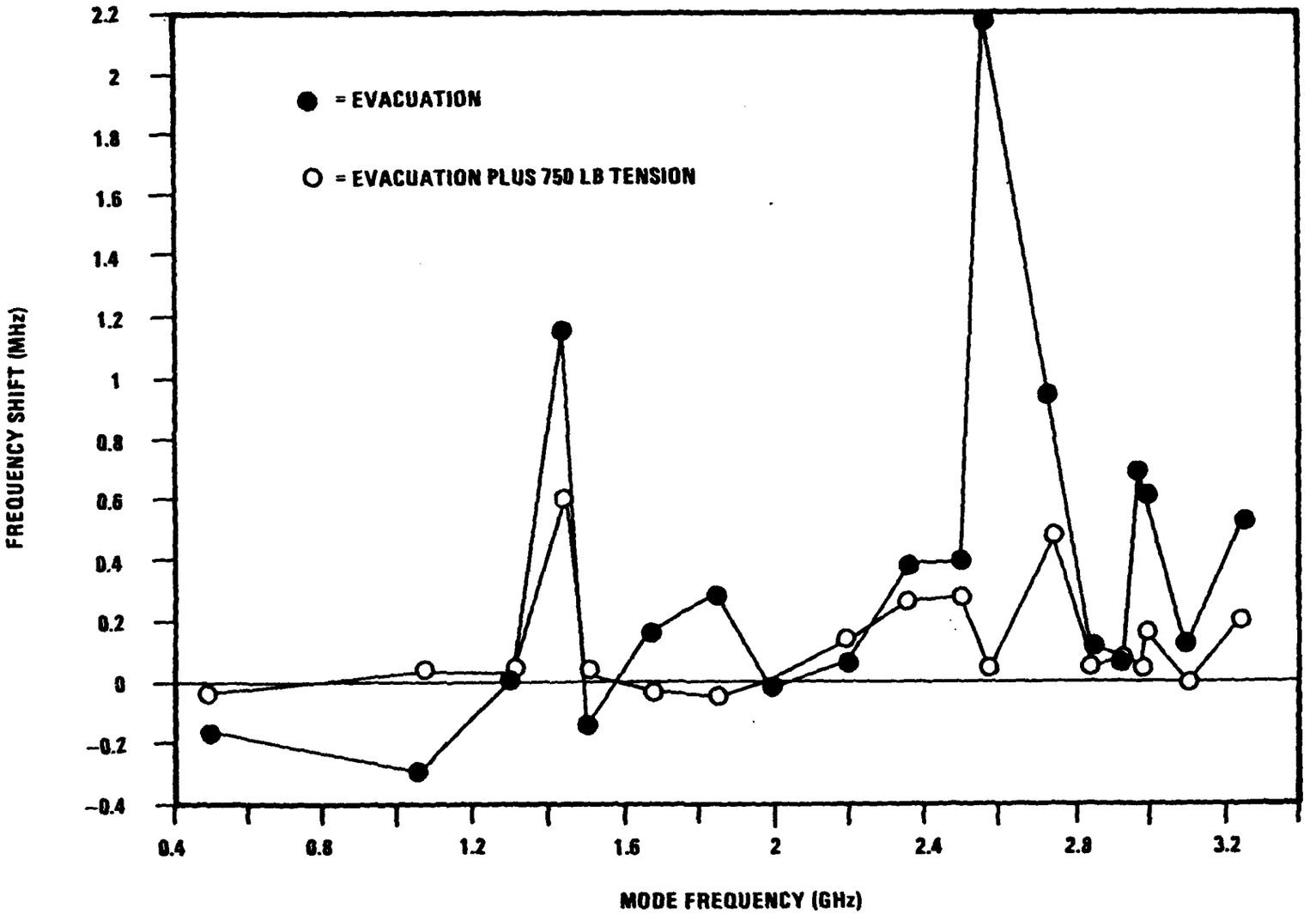

FIGURE 2-5: Frequency Shifts of Modes Frequency Shifts of First Twelve Symmetric Monopole Modes Under Cavity Deformations Shown in Figure 2-3.

the first few symmetric monopole modes. Because the field structures of the modes vary, the geometry change will cause either positive or negative frequency shifts of varying amounts. The magnitude of this frequency shift is important because in principle it is possible for a HOM to come into resonance as the frequency of the fundamental mode is altered, growing to a very large amplitude and interfering with the beam.

2.3 WAKEFIELD AND HOM GENERATION

As a single electron bunch encounters a variation in the radius of the beampipe (i.e., the cavity), electromagnetic fields (wakefields) are generated, some of which evanesce and some of which are supported by the cavity even after the charge bunch has left the cavity. These fields act on the exciting bunch (while it is present) and on the following bunches. See Figure 2-6. Driven by a periodic electron beam, the fields can add coherently. The problem can be broken into single bunch and multibunch effects. Perscriptions for minimizing the excitation of these HOMs are presented.

2.3.1 Single Bunch Effects As the bunch traverses the cavity, a wake potential forms. The amplitude of the wake and its axial extent depend on the shape of the bunch and the total charge. This problem was analyzed with the code

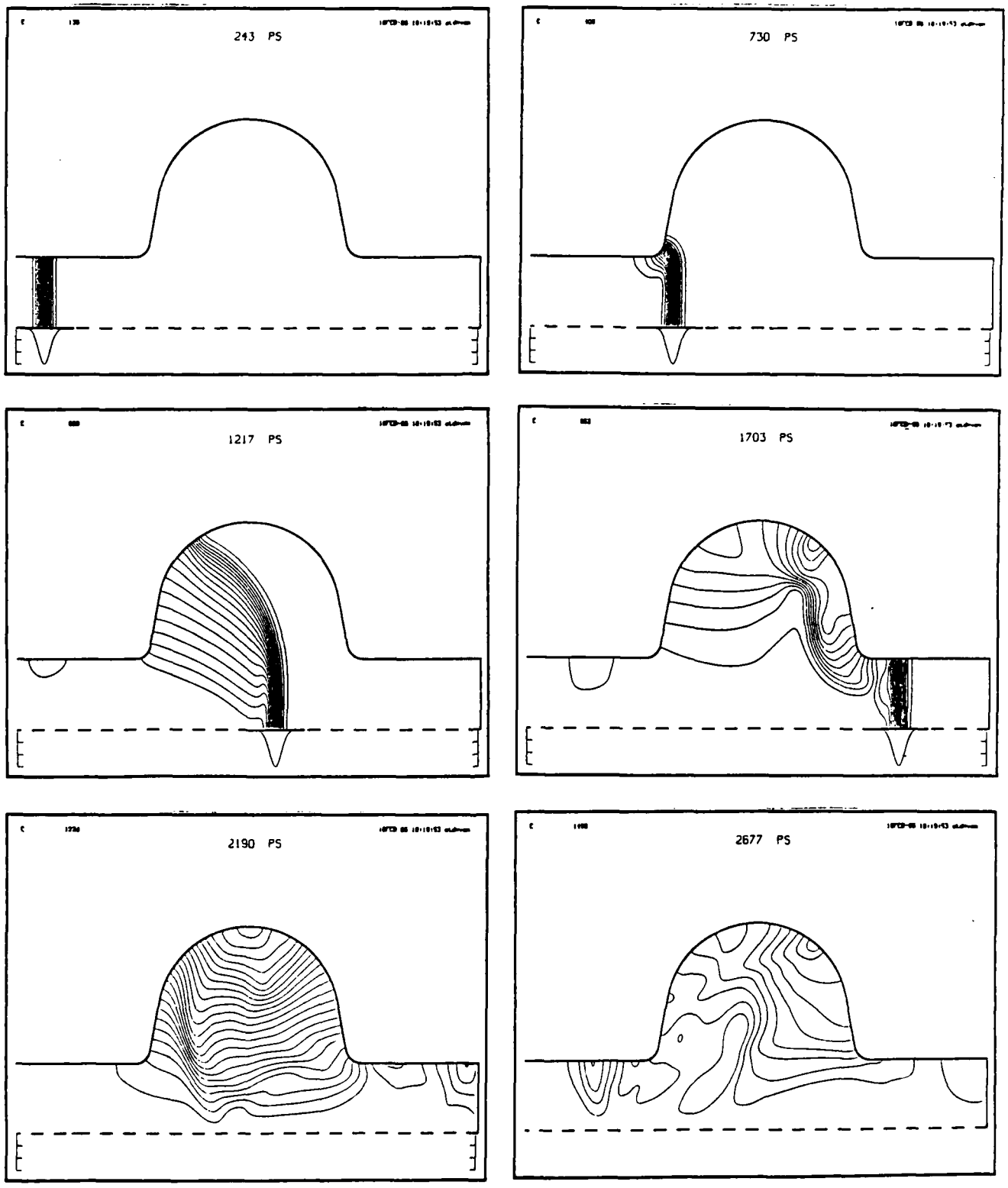

FIGURE 2-6: Wakefield Generation by a 30 ps Bunch. The Location and Profile of the Beam are Shown Below the Dashed Lines.

TBCI. A typical result is shown in Figure 2.7. A voltage droop appears across the length of the pulse. As the charge is stretched over a long pulse the amplitude of the droop is reduced. The indication is that in order to minimize energy spread in a single high charge bunch, a long micropulse is desired. The same energy spread is added by each cavity the beam traverses.

2.3.2 Multibunch Effects As more bunches follow, the fields from each bunch add to those of the previous bunches.This is a classic problem in accelerator physics. The result is that the voltage of some cavity modes will grow to a point where they can affect the beam appreciably while others will be depressed. Whether any given mode is in fact dangerous depends on the specifics of how the whole accelerator is run, i.e., bunch length, interpulse spacing, macrobunch length, charge per bunch, external loading, etc.

Which modes grow depends on the phase of the arriving bunch relative to the phase of the mode and the interbunch spacing normalized to the mode decay time. Enhancement over the single-bunch induced voltage occurs when the freqency of the mode is sufficiently close to a harmonic of the bunch arrival frequency, which is a subharmonic of the accelerator frequency. Considerable care should be taken to ensure that these modes are not excited.

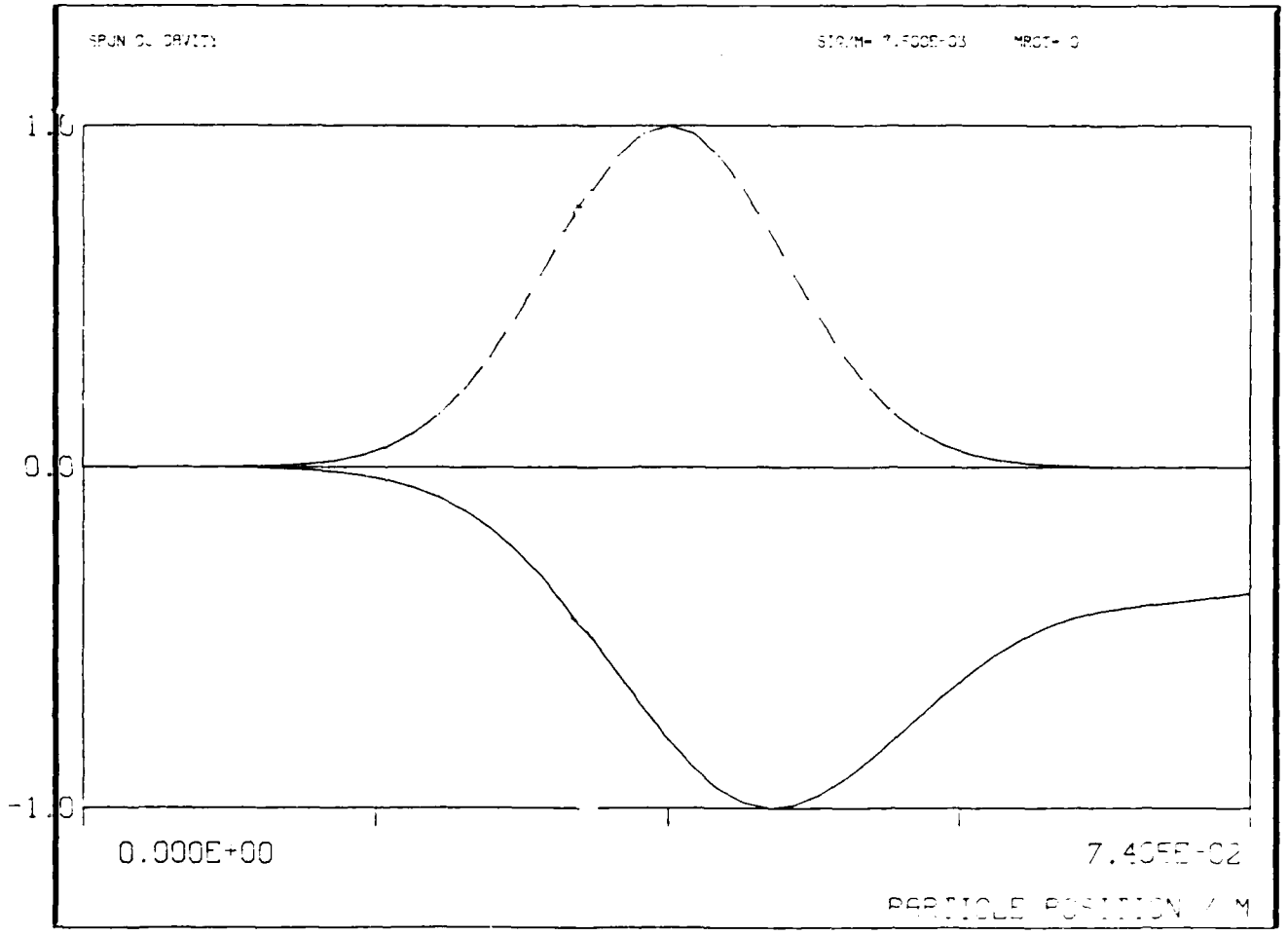

FIGURE 2-7: Wakepotential Trailing a 60 ps Bunch.

2.3.3 Consequences of Subharmonic Bunching One outcome of this analysis is that subharmonic bunching increases (by the subharmonic number) the chance of hitting a resonance, although the voltage enhancement is reduced by the same number. In a statistical sense, subharmonic bunching should be avoided to reduce the number of excitable modes.

2.3.4 Mode Control Using Bunch Shape The density of longitudinal modes per unit frequency in the cavity goes as the frequency. Some mechanism to limit the number of potentially troublesome modes to a managable number must be used. One knows that as the frequency increases the R/Q of the modes appraoch zero. However, the rate at which the R/Q's decrease is imporant. URMEL calculation shows modes with appreciable R/Q out to 10 times the fundamental frequency, so this argument cannot be relied upon. One could assume that all modes above cut-off propagate out of the cavity, reducing the Q. As shown earlier trapped modes exist, which violates that argument. Finally, one can use long, smoothly varying bunches to limit the induced voltages. A bunch with a temporal structure of $\exp(-t^2/2T^2)$ excites only frequencies below $f_{max} = (\sqrt{2}\pi T)^{-1}$. Again, this indicates that the bunch length should be as long as possible.

2.4 OPTIMUM BUNCH LENGTH

Although wakefield, HOM excitation and space charge effects all drive the optimal bunch to longer lengths, the time dependence of the RF acceleration process pushes toward short bunch length. The energy gained by an electron injected off the peak of the acceleration curve is less than that gained by the on-peak particle, leading to a length-dependent energy spread. In addition, the azimuthal magnetic field passes through zero so the local emittance ellipse rotates in opposite directions on either side of the reference electron. Although the instantaneous emittance is unchanged, the axially-averaged emittance grows. Both of these RF dynamics effects have been modeled extensively using the code PARMELA, including finite space charge.

The conflict is resolved through the use of harmonically-related cavities.[5] This essentially synthesizes a square wave electric field. A longer bunch length can be accommodated while still minimizing energy spread. The radial forces that cause emittance growth are also greatly reduced. These improvements are illustrated in Figure 2-8.

2.5 RELATED WORK

In addition to installing the codes URMEL, TBCI, and PARAMELA, the code TRANSPORT was obtained and modified to include focusing effects from standing wave cavities. (The code originally treated only travelling wave structures.)

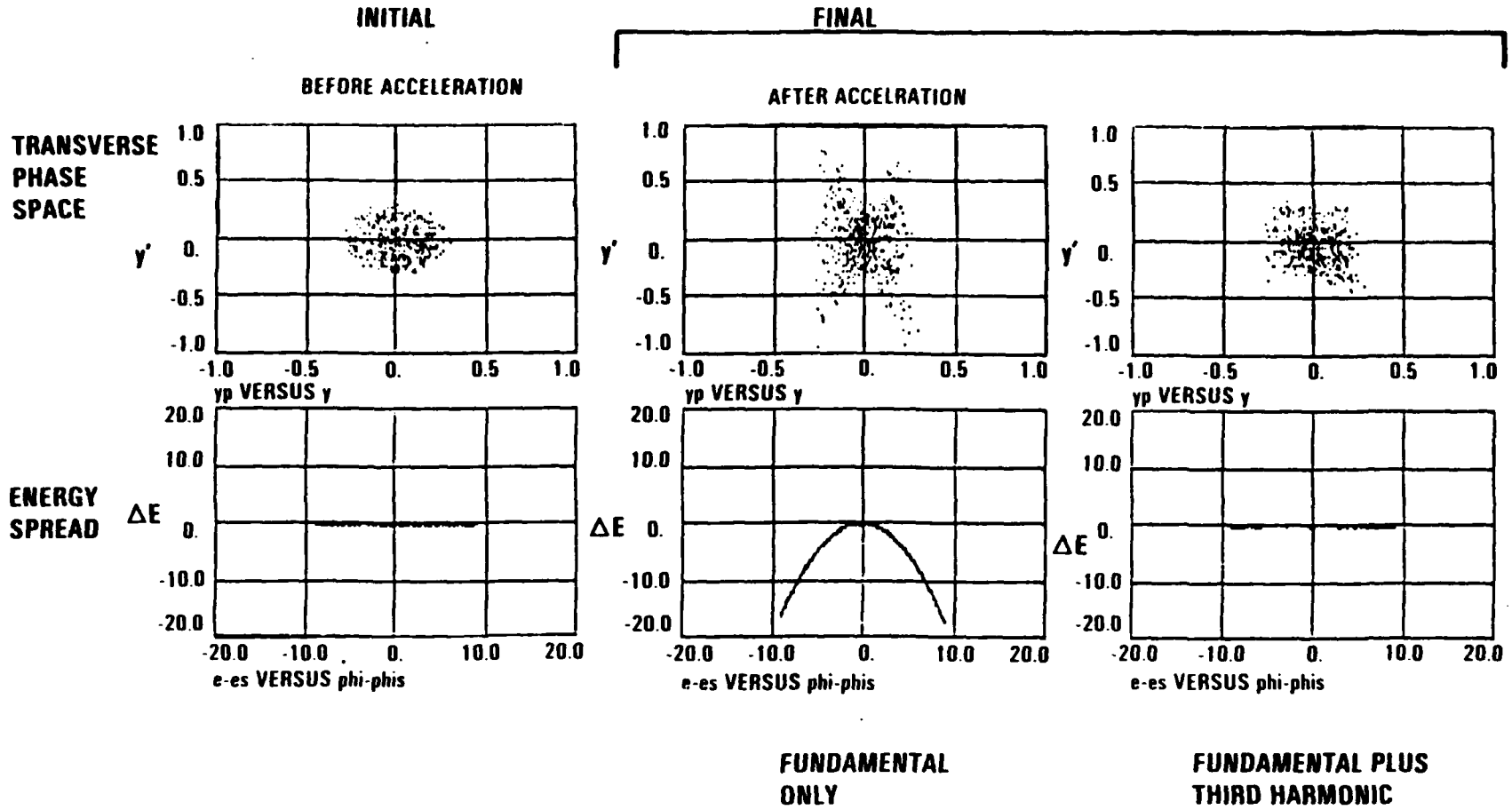

FIGURE 2-8: Harmonic Acceleration Permits Long Bunches. Energy Spread and Emittance Growth are Minimized.

This addition allows the inclusion of the cavities into the beamline design of an accelerator.

3.0 PHYSICAL MODELS AND TESTS

Full-size models of the cavity, the high power coupler and the higher order mode couplers were constructed. Measurements were made to compare with predictions (where applicable) and to serve in place of predictions when numerical modeling is not sufficiently accurate. The work included: developing measurement techniques for isolating the "important" modes from all the others; making mode measurements on the cavity relavent to accelerator physics questions; designing an appropriate high power (HP) coupler and testing the coupling to the fundamental mode; and designing an appropriate higher order mode (HOM) coupler and testing the coupling to the HOMs.

3.1 DIAGNOSTIC DEVELOPMENT

During the design phase of the cavity, a method for characterizing all important cavity modes (m=0,1,2) was developed. Although they were not the fundamental limitation, time and equipment availability restricted the measurements to frequencies below 4 GHz (8 times the fundamental frequency). This is over four times higher in frequency than cavity measurements are traditionally made. Accelerator designers usually worry about suppressing only the strongest modes, but the high average currents needed will excite weaker modes as well. The diagnostic test stand and the method are described in this section.

3.1.1 Aluminum Cavity A simple cavity system was chosen for diagnostic development. The basic geometry was that of a right circular cylinder with beam pipes. The 500 MHz cavity was constructed from 6061 aluminum alloy. The cavity radius was 23.6 cm and the length was 25.0 cm; each beam tube length was 15.0 cm and the radius was 9.0 cm. Eight access holes for diagnostic probes were drilled in the equator at 45^{o} intervals; the end plates had holes drilled through the axis.

3.1.2 Symmetry Properties The cavity is azimuthally symmetric (in the absence of couplers) and symmetric about the axial midplane. The allowed modes can be classified as having a specific mode number and as being either symmetric or antisymmetric in z. In analogy to a right circular cylindrical cavity, the modes can be classified as TM-like or TE-like. (The beam tubes break the symmetry).

At the cavity end walls and equator, the modes have specific field properties that allow them to be easily distinguished from other modes. For example, antisymmetric monopole TM-like modes have E_r= constant and H=0 on the equator. Phase information contained in the field may also be utilized.

3.1.3 Mode Selectivity A single probe on the equator will launch or detect any mode of a given axial symmetry, irrespective of azimuthal or radial mode number. Because the number of modes of interest is large, it is desirable to excite and detect only specific m-value modes. This is done by placing matched probes symmetrically around the equator and driving them with the proper phases, using a single source and power splitters and 180° hybrid couplers. For example, consider four probes placed 90° apart around the equator. Driven in phase, they will produce only m=0,4,8,... modes; if two adjacent probes now have their phases switched 180°, m=1,3,5,.. modes are generated. If probes opposite to each other have the same phase, but are opposite to the remaining two probes, then m=2,6,... modes result. Similar configurations can be used to combine the signals from the other four prbes, thereby doubly discriminating against unwanted modes, both in excitation and detection.

Figure 3-1 demonstrates the advantage of using selectivity in isolating modes with specific m-values. The top trace shows a scan of the ratio of transmitted to incident power versus frequency, using just one launch probe and one detection probe. The lower traces show the same frequency range, but selectivity has been used to substantially reduce the sensitivity to undesired modes; 20 to 40 dB of supression is typically achieved. A larger

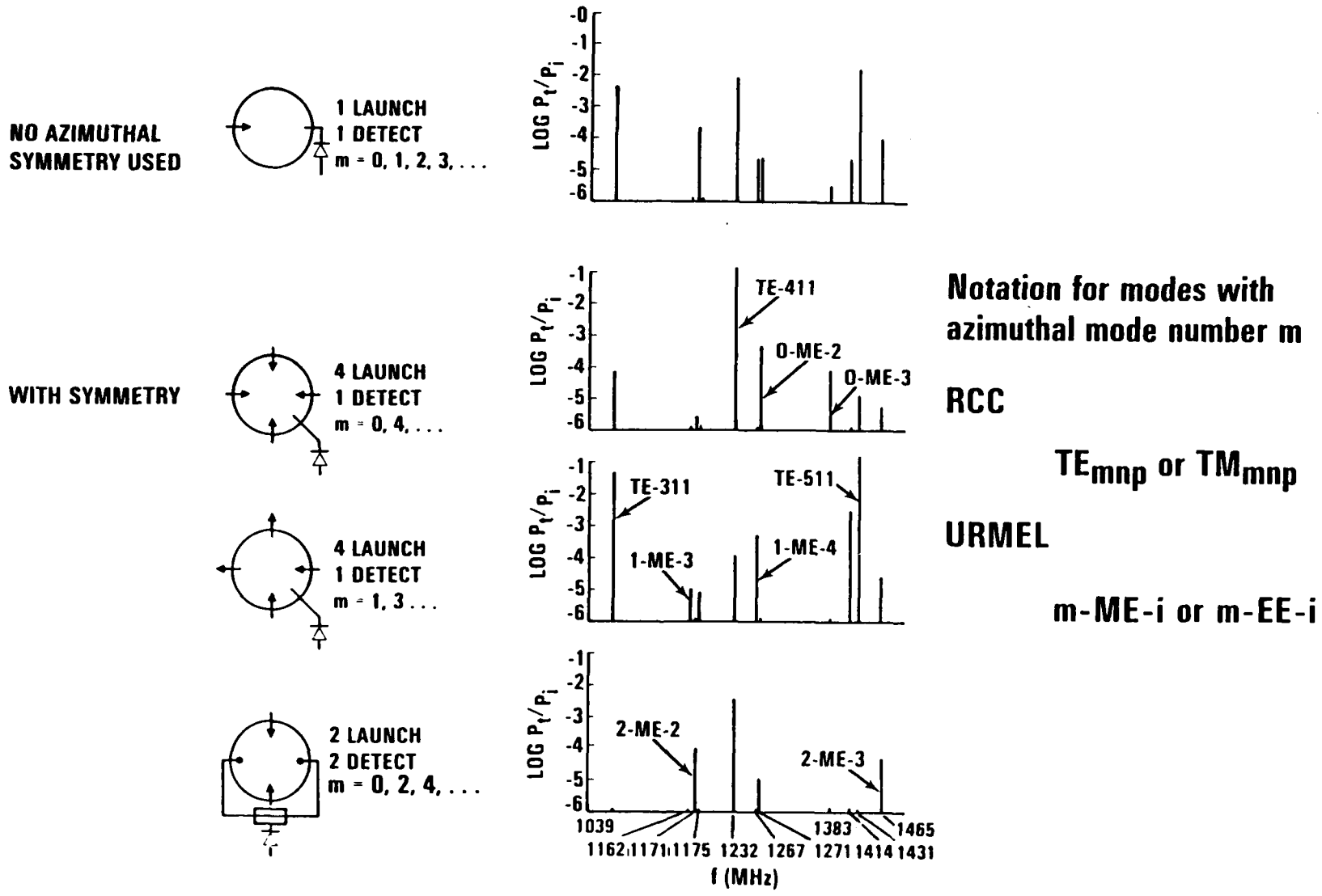

FIGURE 3-1: Selectivity Based on Symmetry Properties Aids Mode Identification and Isolation.

number of probes around the equator would allow discrimination against higher m-values as well.

3.1.4 Data Acquisition A semiautomatic data acquisition system was developed and bench tested. In this system, power at a specific frequency is generated by a computer-controlled frequency synthesizer and fed to a single probe on the equator. Resonance is monitored by transmission to a probe on the opposite side of the equator. The computer is rapidly stepped in frequency and pauses only when the monitor probe power level exceeds a threshhold level, indicating the beginning of a cavity resonance. The power to all the other probes is then digitized and recorded, along with the input freqency. This recording continues until the monitor prove signal falls below threshold, indicating the end of resonance. The frequency then rapidly advances to the next resonance. Data is stored on a floppy disk for later analysis.

Figure 3-2 is the type of data that is obtained. The top graph shows the predicted antisymmetric monopole mode spectrum and amplitude. The center graph shows the modes actually measured in the closed cavity. The bottom graph shows the measured mode spectrum in the same cavity, but with matched loads replacing the end walls. Note the existance of two trapped modes above the waveguide cutoff frequency.

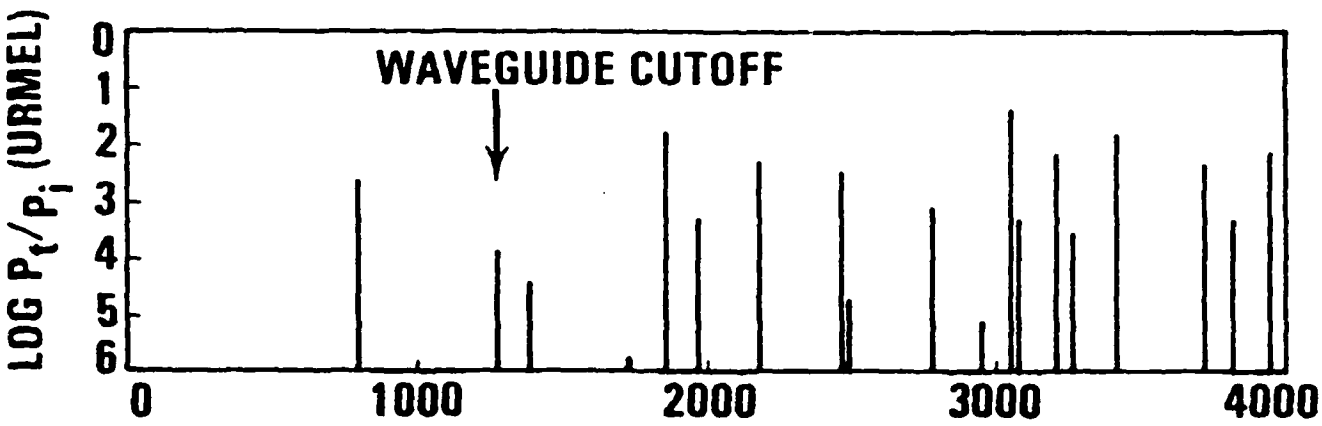

(a) URMEC Predictions

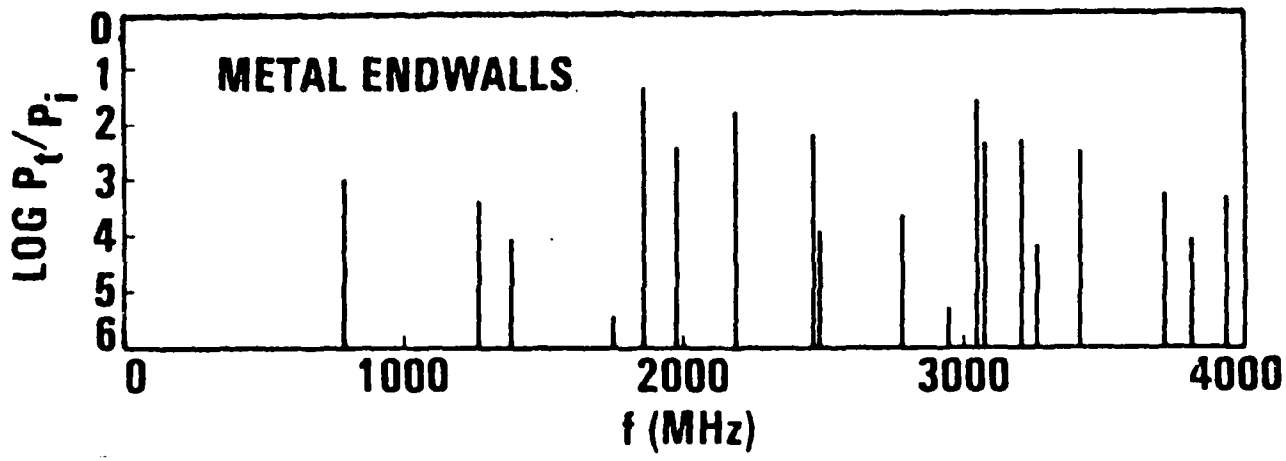

(b) Closed Cavity

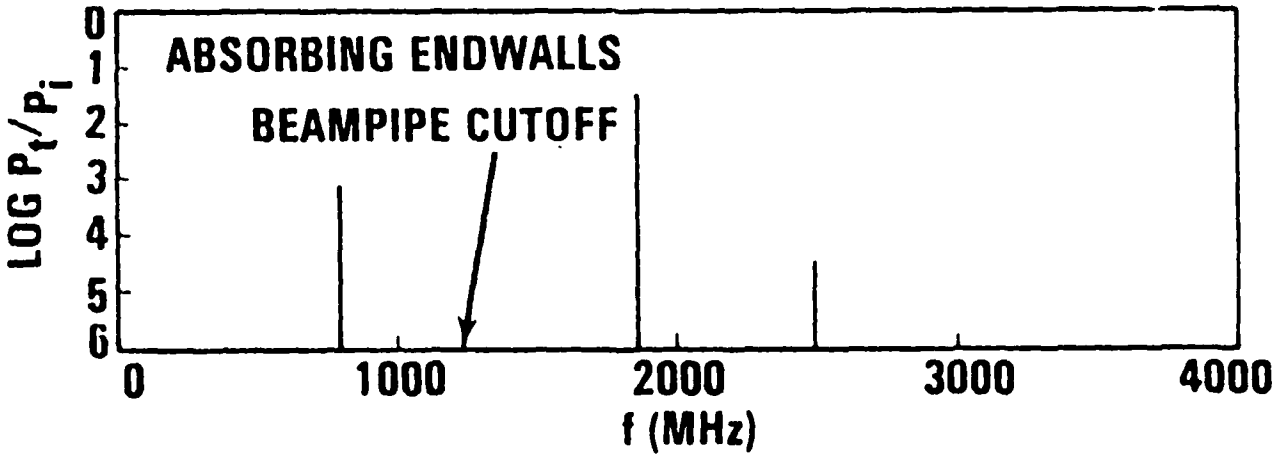

(c) Open Cavity

FIGURE 3-2: Antisymmetric Monopole Modes in Aluminum Cavity.

3.2 COPPER CAVITY

Two full-size copper models of the niobium cavity were built based on the optimized shape shown earlier [Figure 2.1(b)]. One cavity has simple beam pipes, the other has beam pipes with ports for coaxial high power and higher order mode probes.

3.2.1 Fabrication The hemispherical domes of both cavities were formed by spinning 1/8" thick copper sheet onto a form. The domes were trimmed and had welding lips machined into them. Before brazing, the cavities were assembled and the fundamental resonance in each was measured; the frequencies differed by only 0.5 MHz out of 500 MHz. The cavities were brazed. Diagnostic probe ports, similar to those on the aluminum cavity, were added. The interior of the cavities were cleaned. Figure 3-3 is a photograph of the cavity with probe ports.

3.2.2 Cavity Modes As with the aluminum cavity, the modes of the closed copper cavity were measured, classified and compared to URMEL predictions. Once again, the existance of trapped (high Q) modes above cut-off was verified by measuring the modes both with and without a matched-load absorber. The trapped modes are listed in Table 3-1. Longitudnal modes near harmonics of the fundamental frequency are listed in Table 3-2.

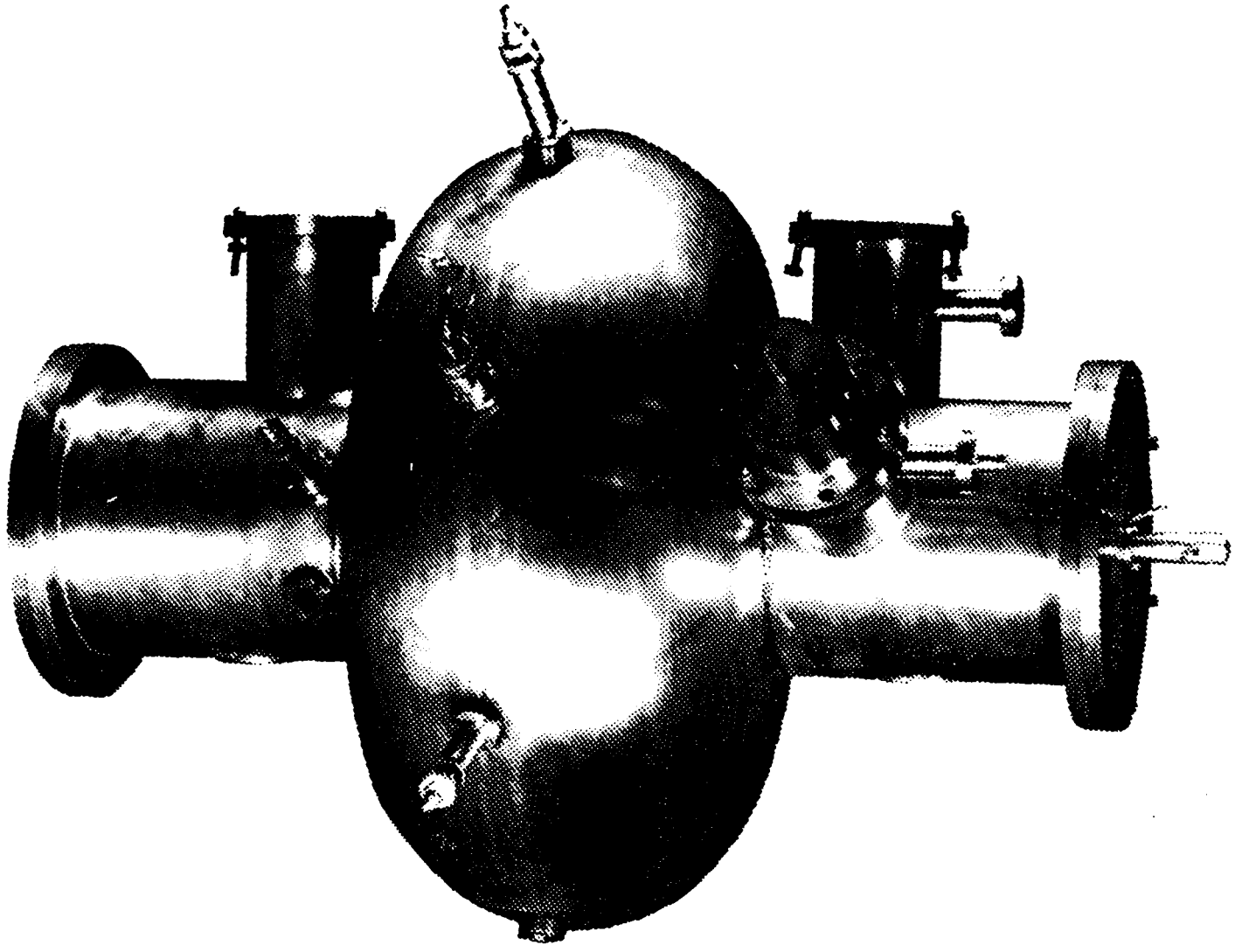

FIGURE 3-3 Full Scale Copper Model of Cavity with Coupler and Diagnostic Probes.

MEASURED FREQUENCY	MODE NUMBER	AXIAL SYMMETRY	URMEL FREQUENCY
501.4	0	S	499.6
675	1	A	671
724	1	S	724
893	2	A	889
926	0	A	914
974	2	S	974
1063	0	S	1061
1273	2	A	1266
1397	2	S	1389
1415	2	A	1413
1496	2	S	1485
2312	0	A	2278
2291	2	S	2324
2570	2	S	2550
2594	0	S	2578
2877	0	S	2845
2998	1	A	2975

TABLE 3-1: TRAPPED MONOPOLE, DIPOLE AND QUADRUPOLE MODES

ASSUMMING EVERY RF BUCKET IS FILLED:
5 MODES WITHIN .3% OF HARMONICS

ASSUMING EVERY FIFTH BUCKET IS FILLED:
11 MODES WITHIN .3% OF HARMONICS

ASSUMING EVERY TENTH BUCKET IS FILLED:
24 MODES WITHIN .3% OF HARMONICS

TABLE 3-2: MONOPOLE MODES NEAR HARMONICS OF BUNCH FREQUENCY

3.2.3 Mode Axis Commonality For a linac built of single-cell cavities, it is possible to steer the beam so that it minimizes the amplitude of a particular dipole mode in each cavity. In such a situation the beam traverses the mode's electromagnetic axis in the cavity. If all dipole modes in a cavity have the same axis then beam breakup could be greatly suppressed by this technique. A measurement was made to determine the location of the mode axes of two dipoles in the cavity with coaxial probe ports. The axes coincided to within the experimental error of 0.5mm.

3.3 HIGH POWER COUPLER DEVELOPMENT

Following the work at CERN,[6] a coaxial 50 ohm coupler was designed. The reason for modifying the CERN design is concern over the long cryogenic lines extending above the cavity and the positional stability (and therefore coupling stability) of the probe. A simplified model of the probe was built and the coupling tested. The coupler is shown schematically in Figure 3-4

3.3.1 Coaxial High Power Coupler Design The primary modifications are in the cryogenic design and the choice of materials. The inner conductor is stainless steel tubing, not niobium, and it is cooled with liquid nitrogen, not helium. The tubing is coated with .001" of copper for improved electrical conductivity. Another modification to

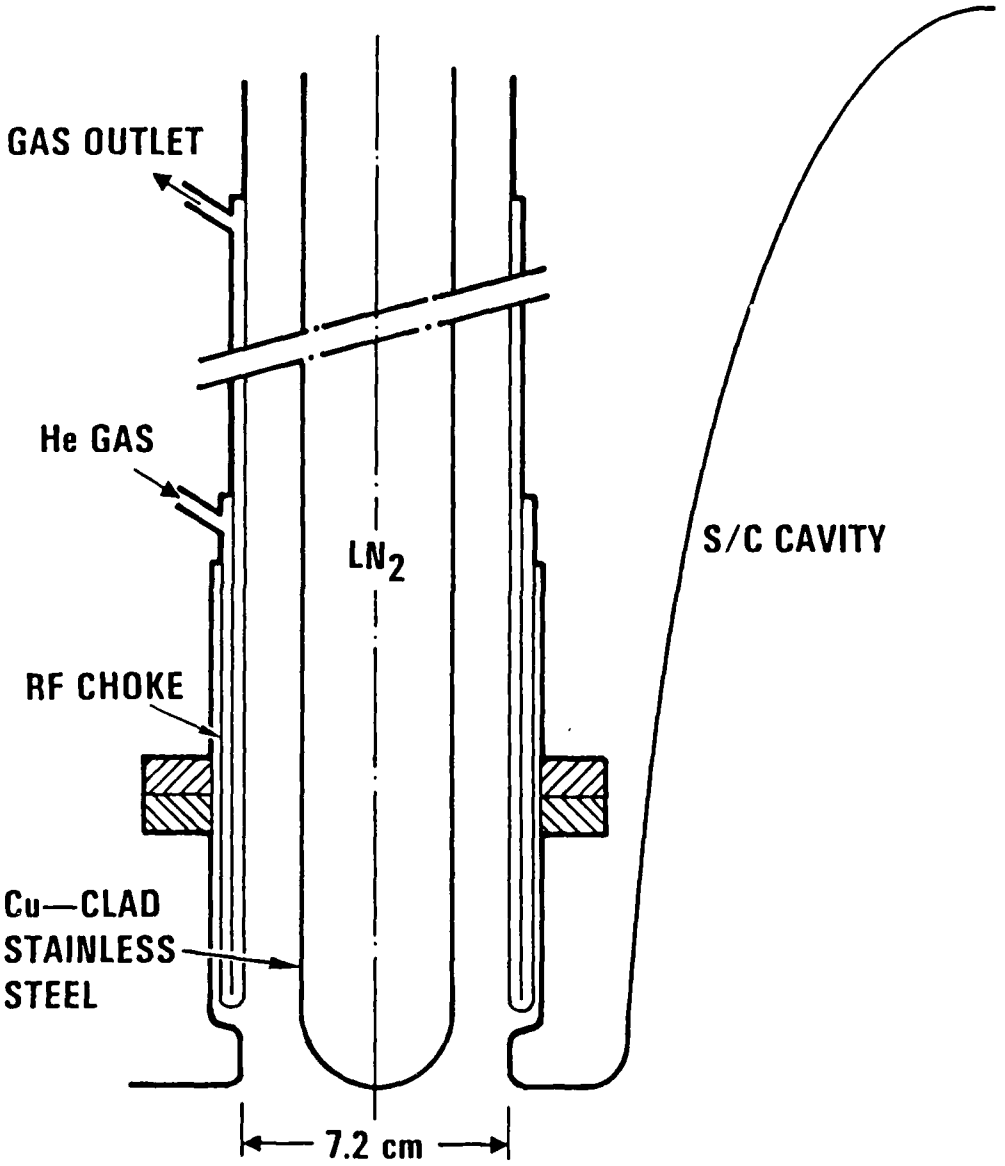

FIGURE 3-4: High Power Input Coupler

the CERN design was to change the probe tip from a flat to a hemisphere. This was done to reduce the peak field at the at the probe tip, although this reduces coupling strength for a given probe insertion. A flat with radiused edges would be a good compromise. As in the CERN design, the vacuum seal is made in a coax-to-waveguide transition, using a cylindrical window. Window tests at CERN have shown that at least 170 kW cw can be coupled.

Although our design is considerably more compact and vibrationally stable, it does require a LN_2 source (for 200 kW coupled into the cavity, 2 l/hr of LN_2 is boiled in maintaining the probe at 77 K) and it presents an additional 1 W to the static dewar heat load.

3.3.2 High Power Coupler Tests A full-size model of the coupler was built of stainless steel with the intention of testing the RF and mechanical properties of the coaxial coupler. The coax-to-waveguide transition was not constructed.

Transmission measurements made on the copper model of the cavity yielded a $Q_{coupler}$ of 2.5×10^7, as measured from the RF source. This is a factor of 100 less coupling than the requirement listed earlier. There are several factors contributing to this. Foremost, there was a large mismatch

due to the absence of an adequate RF source-to-coupler transition; most of the incident power was simply reflected at the source-coupler interface. Also, the coupling port was further from the cavity than it could have been, so the fringe fields which couple the cavity and the probe were weaker. Finally, the probe tip was rounded rather than flat, again reducing the coupling to the fringe fields. These problems can easily be rectified in future work.

3.4 HIGHER ORDER MODE COUPLER DEVELOPMENT

Coaxial probes on the beampipe immediatly adjacent to the cavity are the prefered method of coupling the HOM power out of the cavity. The probes must be sufficiently close to the cavity couple to trapped modes. Since coaxial probes can also couple to the fundamental mode, they must have some method to keep all the fundamental power from travelling up the transmission line to the dump. Such a probe was designed and tested. The proper orientation of the probes for maximal coupling to all important modes was determined and implemented in the cavity design. A method for providing further damping of the propagating HOMs was also investigated.

3.4.1 Probe With Integral Filter Rather than a simple probe followed by a complex filter, a coupler was built along the lines of those developed at CERN.[6] The device, shown in Figure 3-5, can be viewed as a lumped-parameter

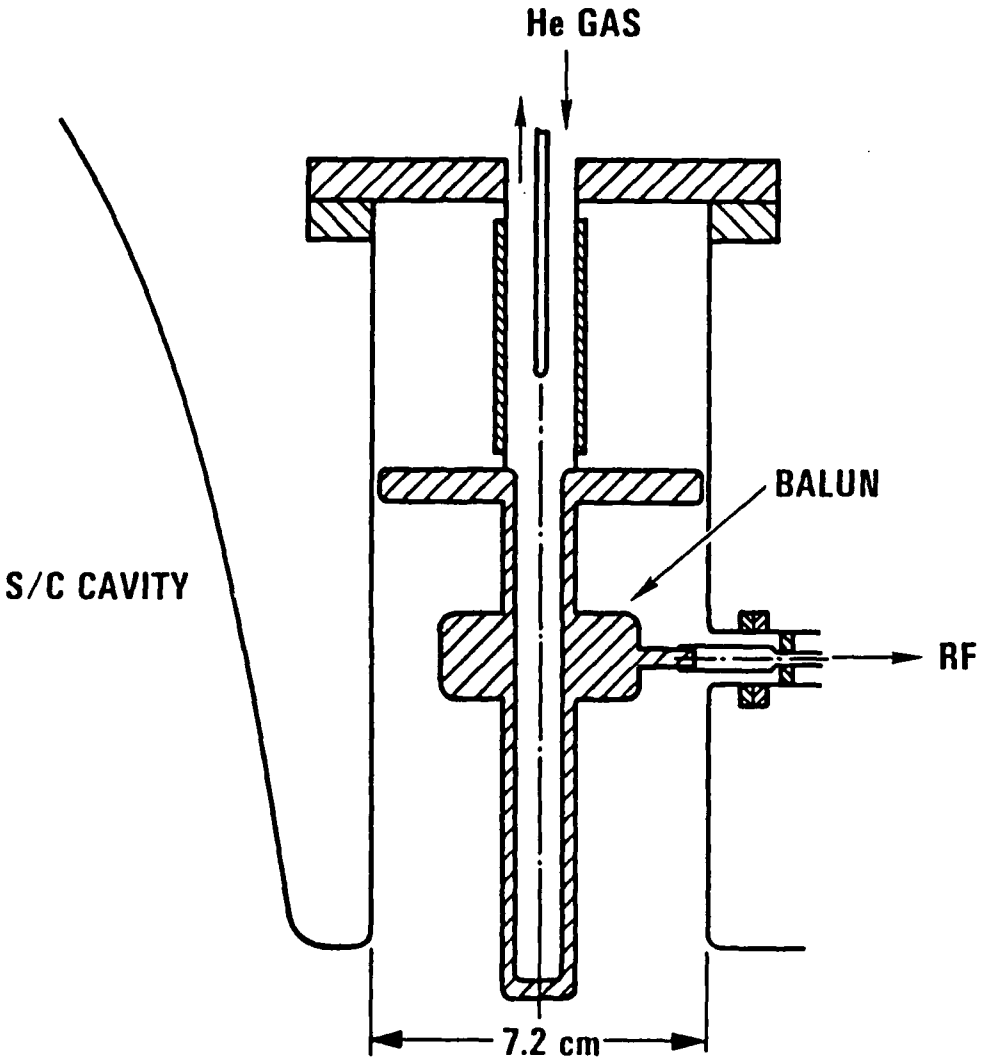

FIGURE 3-5: Higher Order Mode Coupler with Filter

circuit, with the disk forming capacitors and the post between them acting as an inductor. AT 500 MHz, the voltage on the lower disk is nulled; thus no power flows along the 50 ohm cable to the external load. At other frequencies the voltage is finite and power flows.

A model of this probe was built and its transmission characteristics were measured. The transmission characteristics of the probe were qualitatively similar to CERN's published data. A positive feature about this design is that there are no additional notches at higher frequencies. The depth of the single notch was about 50 dB. The measured notch frequency on this probe occurred at 460 MHz; although it was not deemed necessary for these tests, the frequency can be tuned by shaving the upper disk (trimming the capacitor).

The $Q_{external}$ of the probe varied from mode to mode, with a minimum of 2×10^4 and a maximum of 6×10^6. The coupling could be varied to some degree by putting extensions on the probe tip, but this moves the notch around in frequency as well. The degree of coupling cannot be readily changed since the coaxial side port prevents the probe from being moved in or out. Additional work will be necessary to produce a design with a significantly lower external Q.

Although the design indicates a flanged, demountable probe, in practice a high power HOM coupler would probably be welded in place. A resonant choke (similar to that used for the high power coupler) would not be feasible because the HOMs cover a wide range of frequencies. A solid connection would be necessary to avoid ohmic losses at vacuum seals.

3.4.2 Optimum Probe Orientation Probes are typically separated azimuthally about the beam pipe by 90^{o} to couple to both dipole polarizations. However, for high average currents, quadrupole modes could also cause problems (beam astigmatism). Probes oriented at 90^{o} will not couple to one of the quadrupole polarizations. Orienting the probes at 70^{o} allows strong coupling to both quadrupoles while only degrading the dipole coupling by 25%; this feature was incorporated into the cavity design.

3.4.3 Beam Pipe Absorbers A preliminary investigation was made into lining the beam pipe with volumetric microwave absorbing material between cavities to further damp the propagating modes. This would entail bulging the beam pipe (gently, to prevent further HOM generation) and filling the bulge with a lossy dielectric. Impinging waves would reflect only weakly at the interface and be absorbed as they propagate. This work is in a conceptual design phase; the details are still being developed.

4.0 AUXILLIARY SYSTEMS AND INTEGRATION

The configuration of a complete superconducting accelerator module, composed of cavities, tuners, couplers, cryostat, etc., was established. Steps necessary to begin fabrication of a niobium cavity based on the work done in the present contract was initiated.

4.1 BEAMLINE DEWAR

A preliminary dewar design is shown in Figure 4-1. The dewar holds two cavities, each with independent RF feeds. The HP couplers are separated by 40 cm, for a total of 80 dB isolation between the cavities; the two cavities are uncoupled. The HOM couplers are shown, along with their coaxial feeds to the outside. Each cavity has a tuner, driven by a cold motor and PZTs. Liquid He is fed from the bottom, gaseous helium is bled from the top. Multiple dewars may be linked cryogenically. The heat shield is cooled with gas. The length of the dewar is driven by the need to keep the heat conduction low and the need to come to room temperature between dewars (for RT beampipe absorbers, the insertion of beam diagnostics, focussing and steering magnets, etc.) Estimated static heat load (to 4.2K) is about 8 watts.

4.2 PROCESSING FACILITY DEVELOPMENT

A number of steps have been taken to prepare for fabrication and test of superconducting cavities at TRW.

4.2.1 Niobium Procurement Enough high purity niobium sheet was purchased to fabricate two 500 MHz cavities. The material has a residual resistance ratio in excess of 100.

4.2.2 Chemical Processing The chemical processing steps necessary to clean the niobium were tested using a machined X-band cylindrical test cavity. The cavity was repeatedly cleaned and tested for Q. With each cycle, the Q improved as the machine-damaged surface was etched away. Mass loss rates agreed with published values.

4.2.3 Diagnostics A thermal mapping system was built and tested. This has become the most common diagnostic for locating defects in niobium cavities. The system is controlled by an IBM PC and produces a graphical representation of the temperature.

4.2.4 Test Dewar A large "soup pot" helium dewar was designed and purchased to perform cold tests of the full-sized cavity. The dewar is large enough to allow horizontal testing of the cavities with power couplers.

5.0 GRADIENT ENHANCEMENT ACTIVITIES AT STANFORD

A superconducting 1300 MHz model of the cavity was fabricated using the new technologies and cold tested. The work is summarized here; a copy of the subcontract final report is included as Attachment A.

5.1 FACILITY MODIFICATIONS

A modular 9' X 12' Class 100 clean room was designed and procured to provide the necessary environment for final cavity assembly. An ultra-purified water sytem for final cavity rinse was also purchased.

5.2 FABRICATION

The cavity was hydroformed using 2 mm thick Stanford grade material. The parts were machined, then electron-beam welded together using the rhombic raster method developed at Cornell. The cavity was chemically cleaned and rinsed.

5.3 TITANIUM TREATMENT

A process similar to the "yttrification" developed at Cornell, was used to purify the niobium. The cavity is wrapped in titanium foil and heated in a vacuum furnace. Interstitial oxygen trapped in the niobium diffuses to the surface where it reacts with the titanium in a "solid-state gettering" process. The titanium oxide is then chemically stripped from the surface and the cavity cleaned again. The

RRR, proportional to the thermal conductivty, increases from 40 to 400.

5.4 DIAGNOSTICS AND PROCESSING

Diagnostics include both thermal mapping and x-ray emission due to electron loading. Helium processing is used to break-in the cavities.

5.5 GRADIENT

Two cavities were made. Both reached accelerating gradients of 8 MV/m.

6.0 CONCLUSIONS

In this program, significant progress was made toward the goal of developing cavity modules for a superconducting linear accelerator to drive a high average power Free Electron Laser. Through a combination of numerical modeling and experimental testing, a cavity geometry was developed that has the desired RF characteristics and that is ammenable to manufacture. Where possible, modifications to existing coupler designs were made to enhance their performance; weaknesses in coupler design were identified and addressed. A compact fully-integrated accelerator module, which could be replicated to form a high power FEL accelerator, was designed conceptually; features included cryostat, cavities, couplers and tuning mechanism. Facilities for fabricating full-size superconducting cavities meeting all technical requirements were initiated. Gradient enhancement tests on superconducting subscale models of the cavity were performed successfully.

The collaboration between TRW and Stanford personnel has proved to be an effective way to achieve difficult technical goals, as evidenced by the success of this program and our tapered wiggler FEL programs. We believe it will continue to be successful in developing high power superconducting accelerator modules for FEL applications.

ACKNOWLEDGEMENT

We wish to thank Dr. Robert E. Behringer for his continuing support of the advancement of Free Electron Laser physics and technology.

REFERENCES

1. J.M.J. Madey, H.A. Schwettman, and W.M. Fairbanks, IEEE Trans. Nucl. Sci., 20, 980 (1973).

2. D.A.G. Deacon, L.R. Elias, J.M.J. Madey, G.J. Ramian, H.A. Schwettman, and T.I. Smith, Phys. Rev. Lett. 38, 981 (1977).

3. J.A. Edighoffer, G.R. Neil, C.E. Hess, T.I. Smith, S.W. Fornaca, and H.A. Schwettman, Phys. Rev. Lett. 52, 344.

4. Ph Bernard, Cavallari, E. Chiaveri, E. Haebel, H. Heinrichs, H. Lengeler, E. Picasso, V. Piciarelli, J. Tuckmanter, Nucl. Instrum. Meth. 190, 257 (1981).

5. T.I. Smith at Lake Tahoe FEL Workshop (1985); and Linear Accelerator Conference at SLAC (1986).

6. E. Haebel, in Proc. of 2nd Workshop on RF Superconductivity (1984).

ATTACHMENT A

Final Report for Subcontract Number P222.DA.84-44569-020

"Design and Development of Superconducting Accelerator Cavities"

A. Cell Geometry: URMEL Calculations and Prototype Measurements

The cell geometry chosen for these 1300 MHz cavity studies is similar to the CERN geometry. As shown in Fig. 1, the side wall of the cavity is sloped at an angle of 10.5° and is smoothly joined to circular sections at the equator and the iris. The most important cavity parameters, as determined by URMEL calculations, are given in Table 1. URMEL calculations have also been done for the 50 lowest frequency m = 0 modes of this cavity. These modes extend to a frequency ten times higher than the accelerator mode frequency. In addition, two prototype cavities of this same geometry have been fabricated from copper and selected microwave measurements have been made. The lowest m=0 modes have calculated frequencies that agree with measured frequencies in the prototype cavities within a few parts in 10^3. At frequencies above the beam tube cutoff frequency only one m=0 mode was found to be trapped. Calculated and measured parameters of all m=0 trapped modes are given in Table 2. Trapping of the TM0-ME-10 mode as one tunes the accelerator mode over the required frequency range will be studied in the future.

B. Cavity Fabrication Techniques

1. Forming

The 1300 MHz cavities were formed out of niobium sheet 2mm thick. Three forming techniques (die forming, hydroforming, and spinning) were considered. Die forming is well suited to fabrication of 1300 MHz cavities but was

Fig. 1: Cavity Geometry and Dimensions

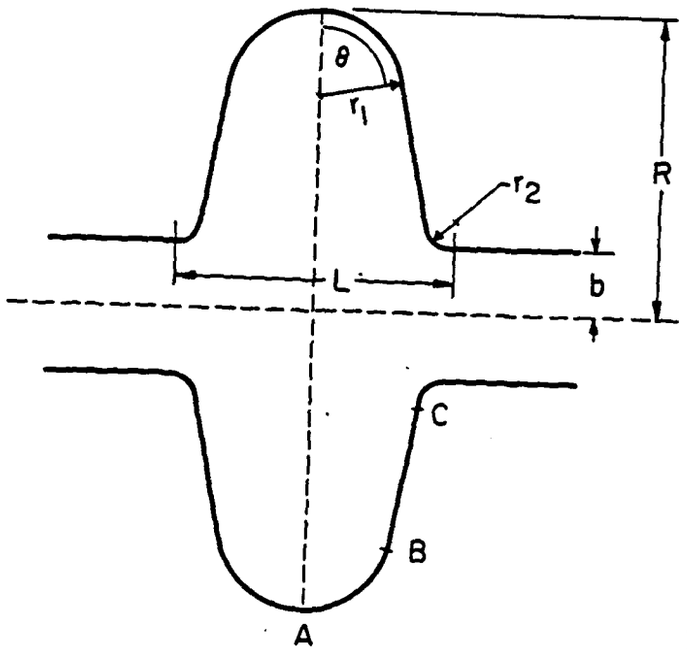

R	10.14 cm
L	11.86 cm
b	6.36 cm
θ	79.5°
r_1	4.56 cm
r_2	1.02 cm

TABLE 1: CAVITY PARAMETERS

For Accelerator Mode with 1 MV Gain Through Cavity

U (Joules)	.481
E_p (MV/m)	15.1
H_p (Alm)	2.66×10^4
R/Q (Ω)	128
Γ (Ω)	261

TABLE 2

COMPARISON OF URMEL CALCULATIONS AND PROTOTYPE MEASUREMENTS

(Trapped m = 0 modes)

Mode	f_{calc}(GHz)	$f_{measured}$(GHz)	Q_{calc}	$Q_{measured}$	R/Q(Ω)
TMO-EE-1	1.2954	1.2966	27740	26500	128
TMO-ME-1	2.3456	2.3515	28050	29000	44
TMO-EE-2	2.7512	2.7567	40163	26100	0.04
TMO-ME-2	3.4817	3.4828	34195	4980	9.0
CUTOFF	3.6083				
TMO-ME-10	7.0729	7.0738	41807	5680	1.0

(Preliminary)

eliminated as an option since it is less appropriate for 500 MHz cavities. Spinning is well suited to fabrication of cavities either at 1300 MHz or 500 MHz but this technique was downgraded because dimensional tolerances that can be achieved are relatively poor. Hydroforming was used because it is an appropriate forming technique either at 1300 MHz or 500 MHz and because better dimensional tolerances could be achieved. For the fundamental accelerator mode and for the lowest frequency higher order modes the resonant frequency of the same mode in different cells was reproducible to approximately one part in 10^3 in the hydroformed cavities. For the niobium sheet used in our experiments we found it necessary to stress-relieve the hydroformed cup at 975°C in a 10^{-5} Torr vacuum in order to maintain roundness after machining off the hydroform lip. The most difficult tolerance to maintain in hydroforming 1300 MHz cavities is the small (0.4") radius in the iris region of the cavity at the junction of the cell and the beam tube. Errors of 10 mils in this region were common but this proved manageable. It is expected that this will be less of a problem at 500 MHz where the radius is larger by the ratio of frequencies.

In establishing an appropriate hydroform cycle it is necessary to carry out a number of hydroform experiments. It was found that annealed Hitachi copper sheet matches the hydroforming properties of niobium (RRR ≈ 150) reasonably well and is a much less expensive material to use in carrying out early hydroform tests.

2. Welding

Joining the hydroformed cups to the beam tube can be accomplished by making an interior weld using a diffuse electron beam. This weld area is machined and polished prior to joining the two cups together at the equator. At 1300 MHz it is not practical to make an interior weld at the equator. The

equator weld is made from the exterior of the cavity using the Rhombic Raster welding scheme developed at Cornell. Under carefully controlled conditions a smooth, full penetration weld can be made.

C. Processing and Assembly

1. Chemical polishing and rinsing

Chemical polishing has been the most commonly used method for treating the surfaces of niobium cavities. The polishing solution consists mainly of hydrofluoric and nitric acids. This solution has to be refrigerated to 0°C to reduce the rate of reaction. Alternatively, the rate of the reaction can be reduced by the addition of phosphoric acid. We use a mixture of equal volume hydrofluoric acid (48%), nitric acid (65%) and phosphoric acid (85%) which removes Nb at a rate of about 10μm/min. Despite the slowing of the reaction, it is still exothermic so precaution must be taken to avoid any increase in the bath temperature. Unfortunately, phosphoric acid has the property of forming water insoluble niobium phosphates on the surface of the cavity, especially when the mixture leaves a film on the warm cavity surface from which hydrofluoric acid and nitric acid evaporate rapidly. Although phosphate formation can be minimized by keeping the draining period as short as possible (less than 1 minute) and by rinsing rapidly with DI water, it is recommended to rinse the cavity in a $H_2O + H_2O_2$ bath with ultrasonic agitation after the chemical polishing to dissolve the remaining niobium phosphates.

Rinsing of the cavity after the final chemical polishing must be done in a closed loop system with high purity dust free DI water. As part of this sub-contract, specifications for this water system were written by Balazs Analytical Laboratory (see attached report) and the system itself was

built by Arrowhead Industrial Water, Inc. After polishing in the closed loop system, the cavity, filled with high quality water, is transported to a clean room for drying and assembly.

2. Drying and Clean Assembly

The cavity, filled with water and protected by covers against dust, is transported to the clean room where the water is drained and the cavity is dried overnight with the assistance of a heat lamp. During drying the cavity is held in an inclined position in order to avoid residues in regions of the cavity favorable for electron field emission and/or electron multipacting. The cavity is then assembled with an indium joint to its support system, kept closed and transported to the experimental area where it is connected to the UHV pumping station.

The clean room where drying and assembly of the cavity occurs was constructed with funds from this contract. Specifications for the room were established by Practicon Associates and the room was constructed by Cal-Air Inc.

3. Titanium purification of niobium

Defects on the superconducting niobium surface of an accelerator cavity lead to thermal runaway or breakdown at some field level. For a given defect this field level can be increased, if the thermal conductivity of the niobium can be increased. Computer simulations of thermal breakdown in cavities show that in the absence of other limiting mechanisms like electron loading the breakdown field is proportional to the square root of the thermal conductivity. The thermal conductivity of niobium at low temperatures is strongly dependent on the purity of the metal i.e. the residual resistivity

ratio (RRR).

Purification of niobium by removing the interstitial impurities (especially oxygen) is particularly important in increasing the RRR, and can be done by external gettering. External gettering is a process whereby a metal which has a higher affinity for oxygen (or N and C) is brought into contact with Nb and acts as a sink for interstitial impurities. Both yttrium and titanium have been used for this purpose. At HEPL we have used this process by vapor depositing a titanium film on the Nb surface. The cavity wrapped in Ti foil is heated to 1300°C in an UHV furnace for 6 hours. At this temperature the vapor pressure of Ti is 7×10^{-6} Torr so that a thin layer of Ti is deposited on the Nb surface. The Ti, which has a higher affinity for oxygen than Nb, traps the oxygen when it diffuses from the bulk to the surface. The diffusion length of oxygen at 1300°C is 3 mm per hour so that removal in 6 hours is very effective. After purification, the titanium is removed by using a nitric-hydrofluoric acid solution containing 18.5% vol HF (48%) 1% vol HNO_3 (65%) and 80.5% vol H_2O. This is followed by a chemical polishing of 2 minutes in the standard solution.

By application of this process, the RRR of standard grade niobium improved from 40 to 400 while the RRR of high thermal conductivity niobium increased from 210 to 560. The RRR obtained in treating the standard grade niobium (400) is higher than that of any commercially available niobium sheet. The RRR obtained in treating commercially available high conductivity material (560) is a world's record for niobium sheet. The high value of RRR attained was due not only to the effectiveness of the Ti treatment but also to the good low base pressure of our ultra high vacuum furnace (10^{-7} Torr).

D. Diagnostic Techniques

1. Microwave

The principal diagnostic techniques used in evaluating cavity performance consist of microwave measurements. The rf energy stored in a superconducting cavity and the peak fields achieved are determined by measuring the power radiated from a monitor probe. The external Q-value of the probe must be independently established. The loaded Q-value, Q_L, of the cavity at the operating field level is determined by measuring the initial decay rate of the rf energy stored in the cavity. The unloaded Q-value, Q_0, can be calculated from the expression $Q_0 = (1 + \beta)\, Q_L$ if the coupling coefficient, β, is independently measured.

2. Electron current and radiation dose

Electron loading in the cavity due either to electron multipacting or electron field emission is monitored by an electric current probe located in the beam tube on the cavity axis. Although probes on the equator of the cavity would be preferable in that electrons are swept outward by the rf fields, the axial probe has the advantage that it does not perturb the cell geometry. Electron field emission is also monitored by measurement of the radiation produced by the cavity. Measurements of the radiation dose and/or measurement of the electric current as a function of the cavity field level shows an exponential dependence that can be analyzed to yield a consistent value of the apparent enhancement (β_a) of the electric field at an emission site.

3. Thermal Mapping

Superconducting cavities are subject to both electric and magnetic defects that limit the accelerating gradient and the cavity Q. Thermal mapping can pin point where heating of the cavity is taking place and therefore localize

defects so that detailed inspection and repair can be done. Also, the location and distribution of heating will tell which type of defect is limiting the operation. Helium processing will reduce electron loading, but thermal breakdown always requires guided repair to improve cavity performance.

Thermal mapping can be accomplished by attaching an array of thermometers to the outer cavity wall. Carbon resistors, used for the thermometers, provide a better sensitivity than 1 millidegree Kelvin at 4.2°K.

The array is electrically connected together in such a way that n electrical leads through the cryostat will monitor $\frac{n(n+2)}{2}$ thermometer resistors. This idea was proposed by Cornell and is very useful in addressing a large array of resistors without a huge number of leads feeding into the dewar. This is achieved by applying a fixed voltage to one lead and measuring the current out of the remaining leads which must be tied to ground. (See Fig. 2a). By sequentially applying the voltage to each lead and measuring the current out of the remaining leads the resistance of each resistor in the array is actually measured twice. In practice, plus and minus voltages are applied to each lead to eliminate thermally induced voltages in the leads. Thus, each resistor is measured four times. The array is set up for 16 leads which gives 112 resistor elements. It takes an IBM PC computer 80μs to read each resistor so that the array can be read in total (each resistor four times) at a 30 hz rate. A sample computer display of the thermal map is shown in Fig. 2b.

E. Inspection

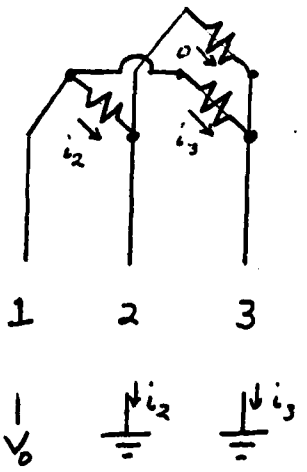

3 Lead Array

figure 2a

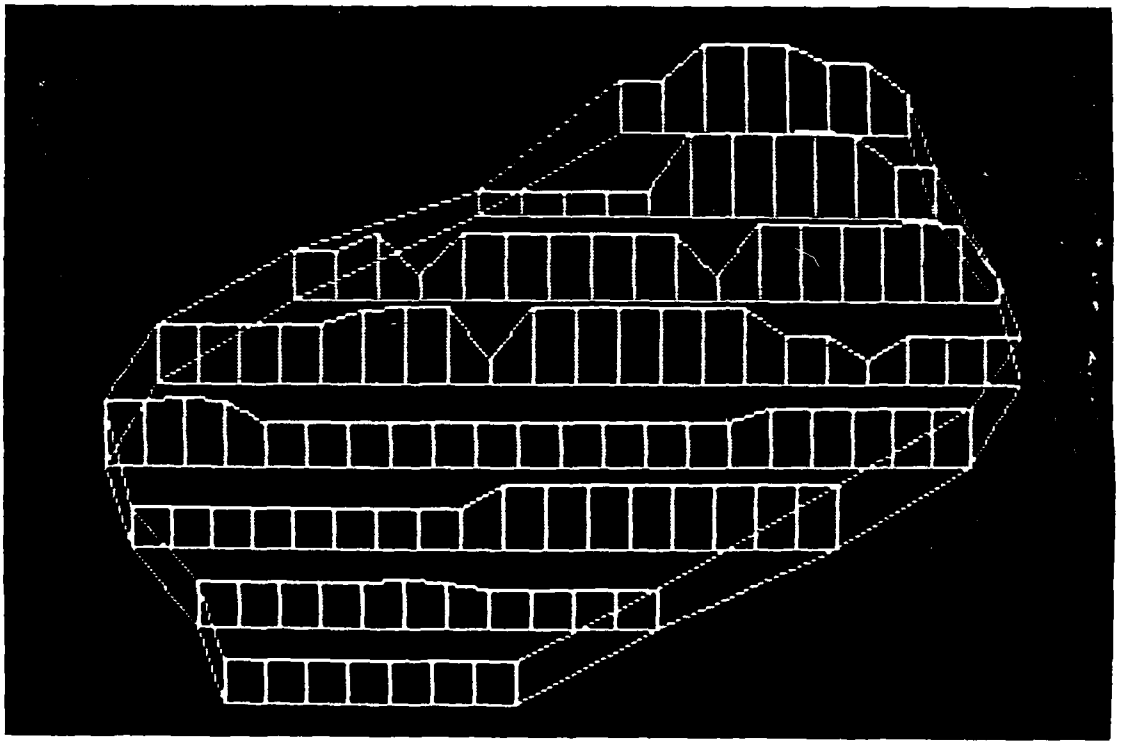

Display of Thermal Map
figure 2b

Every superconducting cavity has on its inner surface defects which limit cavity performance. Some of these defects can be identified at the very beginning of cavity fabrication. Prior to welding, a simple check for iron inclusions at the surface is obtained by immersing the half cells for one night in water. Iron inclusions can then be detected by rust. Other foreign materials can be detected by anodizing the niobium surface. The anodizing technique is based on the principle that an anodic oxide film formed on niobium produces interference colors. The color is characteristic of the anodic oxide thickness which in turn depends on the composition of the substrate. We use an electrolyte consisting of 1 volume of ammonium hydroxide (28%) and 1 volume of water. Voltages around 20 V which give a blue color provide excellent contrast for fine details.

For inspection of the inner cavity surface we have purchased with funds from this contract a Zeiss optical stereomicroscope combined with a first surface mirror. The total magnification obtained with 25 x / 10.5 eyepieces and a long focal objective (f=320 mm) can be varied from 6 to 40. By moving the mirror along the axis of the cavity and by changing its angle with regard to the axis, the whole inside of the cavity can be inspected.

F. Experimental Results

Two single cell 1300 MHz cavities have been fabricated from standard grade (RRR 30) Wah Chang niobium sheet. After fabrication the cavities were chemically polished and rinsed in water. All rf measurements were done in a magnetically shielded cryostat (less than 100 m Oe) with the cavity in a horizontal position. Prior to cool down a vacuum in the range of 10^{-9} Torr was reached.

The experimental results are summarized in Table 3. With standard grade niobium cavities accelerating fields of 5.2 MV/m and 5.1 MV/m were obtained at the first cool down and the level of radiation observed just outside of the cryostat was quite low. These cavities were always limited in field by thermal breakdown due to the low thermal conductivity of the niobium. It is quite interesting to note that these high fields were reached without guided repair (i.e. removal of defects that have been located by thermal mapping techniques) and without helium sputter processing.

The highest Q_0 value achieved at 4.2 K was 3.9×10^8 compared to the theoretical Q_0 of 6×10^8 calculated from the B.C.S. theory. This yields a residual loss Q-value of 1.2×10^9 which was probably due in large part to the short length of the beam pipes (length to diameter ratio of only 1) of our cavities and the resulting losses at the end flanges. No reduction of Q_0 with increasing field was observed for cavity No. 1 up to at least 4.8 MV/m. The Q_0 obtained at 2K was consistent with the residual Q-value determined from the measurements at 4.2K.

The results obtained for the same two cavities after purification of the niobium by titanium treatment were very interesting. In cavity No. 1 the accelerating field reached 6.1 MV/m with a radiation level of 600 mRad/hour and after helium sputter processing for about 2 hours in a pure helium gas atmosphere of 1.2×10^{-4} Torr measured at the warm part of the vacuum system, the accelerating field reached 8 MV/m with only 300 mRad/hour of radiation. In cavity No. 2, a field of 8.2 MV/m was obtained even without helium sputter processing but the radiation level was quite high (2 Rad/hour). The higher fields obtained were due to the increase of the RRR of niobium from 40 to 400.

TABLE 3

EXPERIMENTAL RESULTS OF TWO SINGLE CELL 1300 MHz Nb CAVITIES

CAVITY	SURFACE TREATMENT	T(K)	Q_o LOW FIELD	Q_o HIGH FIELD	E_{acc}^{max} (MV/m)	X-RAY (m R/h)	FIELD LIMITATION
1	Cp (55 μm)	4.2	3.9×10^8				
		2.0	1.4×10^9	1.4×10^9 at 4.8MV/m	5.2	0.6	Thermal Breakdown
1	+Ti + cp (27 μm)	4.2	3.4×10^8				
		2.0	9×10^8	3.7×10^8 at 5.4MV/m	6.1	600	e^- loading
	+ Helium processing	2.0			8.0	300	Available rf power
2	cp (55 μm)	4.2	not measured				
		2.0	1.1×10^9	not measured	5.1	5	Thermal breakdown
2	+Ti + cp (27μ)	4.2	2.6×10^8				
		2.0	1.1×10^9	3.4×10^8 at 8.2MV/m	8.2	2000	Available rf power

As shown in Fig. 3, the Q_0 in the titanium treated cavity (No. 2) degraded from an initial 1.1 x 10^9 at 1 MV/m to 3.4 x 10^8 at the highest field. The reduction of Q_0 with increasing field is thought to be the result of incomplete removal of the titanium. As it is of great practical importance, more work has to be done to see if this effect is inherent to the Ti purification method itself or if it is simply due to insufficient chemical treatment . But even if the first hypothesis is confirmed, one can always use yttrium (which is more expensive) instead of titanium which has been shown at Cornell to yield a more normal behavior of Q_0 versus field level.

G. Approaches to extending cavity performance

Voltage gradients that can be achieved in superconducting accelerator cavities are limited by magnetic and electric defects on the niobium surface. A simple model has been constructed which provides a good qualitative description of the observed behavior of superconducting niobium cavities. It is assumed that the number of magnetic defects per unit area, n_m (H), that will lead to thermal breakdown at a field less than or equal to H is roughly proportional to H^4. For standard grade niobium (RRR ≈ 30) the defect density on a niobium surface is assumed to be approximately 5 x 10^{-4} /cm^2 at a magnetic field strength of 200 Oe (accelerating field ≈ 5 MV/m). It is further assumed that potential emission sites occur on niobium surfaces at a density n_e, of ≈ 3 x 10^{-2} cm^2 and that these are characterized by an apparent enhancement factor of 400.

Let us consider the experimental results described in Section F in light of this model. Since the surface area, A, of a 1300 MHz cavity is roughly 10^3 cm^2 we have: n_m (5MV/m) A (1300 MHz) = (5 x 10^{-4}) (10^3) = 0.5.

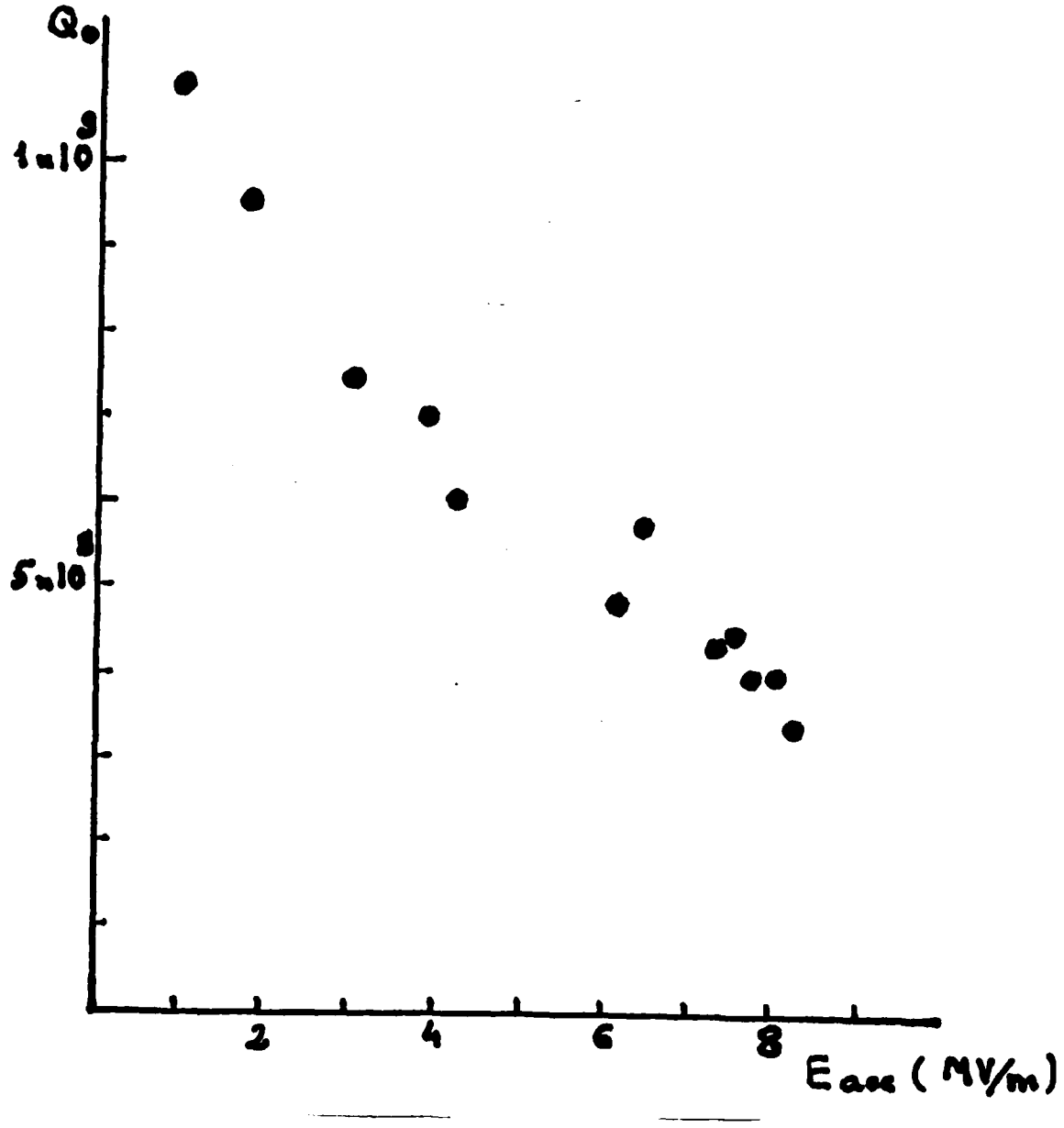

Fig. 3: Plot of Q_o vs. accelerating field of cavity No. 2 after Ti purification.

Thus one would statistically expect that the mean field achieved in a large ensemble of 1300 MHz cavities would be ≈ 5 MV/m. This certainly agrees with the measurements on standard grade niobium cavities reported in Section F. Both cavities were limited by thermal magnetic breakdown and the gradients achieved were ≈ 5MV/m. After treating the standard grade niobium cavities by external gettering with titanium, the RRR increased by a factor of 13 to a value of 400. The magnetic defect that had limited the gradient in the standard grade cavities at 5MV/m becomes stablized due to the improved thermal conduction. To a very rough approximation one expects this same defect to become unstable again at a gradient that is $\sqrt{13}$ higher, i.e. at a gradient of 18 MV/m. To the extent that no magnetic breakdown was observed in the titanium treated cavities this is also consistent with the experimental results described in Section F.

The observed electron loading in our cavity experiments can also be understood in terms of the simple model. At a gradient of 5 MV/m the peak electric field on the cavity wall is 9.5 MV/m. Statistically one would expect a mean field enhancement β_a = 330 for an ensemble of 1300 MHz cavities. This yields an enhanced field value of 3.2×10^9 V/m. Even at 4×10^9 V/m the field emission current and therefore the electron loading will be negligible. This is consistent with the small (mR/h) radiation dose observed in the standard grade niobium cavity experiments. In the titanium treated cavity experiments gradients of 8 MV/m were achieved. At 8 MV/m the enhanced field becomes 5×10^9 V/m and although this is well below the expected breakdown field of 7×10^9 V/m, the field emission current and the electron loading are large. Typically helium sputter processing of niobium cavities is done at an enhanced field of 5.6×10^9 V/m and at this level

radiation doses of a few R/h are observed. This again is consistent with the observed results.

How do these expectations change with frequency? For magnetic defects the mean field level achieved in an ensemble of cavities will vary as $f^{1/4}$. If the mean gradient for RRR = 30 material is 5 MV/m at 1300 MHz, it will be 4MV/m at 500 MHz. To increase the mean gradient at 500 MHz to 7 MV/m one must use material with RRR ≥ 100. Since material of this quality is now readily available, magnetic breakdown of single cell 500 MHz cavities will not be an important problem for operation at 7 MV/m.

For electric defects the situation is more difficult. In a 500 MHz cavity the high electric field area is approximately 70 cm^2 and thus we must expect on average two emitters in this region. Under these circumstances the mean enhancement factor, $\bar{\beta}_a$, will not be much different from 400. At 7 MV/m the peak electric field on the cavity wall is 1.4×10^7 V/m and the enhanced field on the wall is 5.6×10^9 V/m. This field level is readily achieved in superconducting niobium cavities but it is also accompanied by large amounts of radiation. Typically one can expect the radiation level in the vicinity of each cavity to be a few R/h. If lower radiation levels are required one will either have to do extensive helium sputter processing or localize and "surgically" remove emitters from the high electric field region.

In the future it might be possible to achieve gradients of 14 MV/m in single cell 500 MHz cavities. As an isolated experiment this has been accomplished already. The question, however, is whether one can achieve this level consistently. There are good reasons to believe this might be possible. To stabilize the known magnetic defects at this field level will require material with RRR ≥ 400. Our titanium gettering experiments have

already shown this is possible to achieve. The principal remaining issue centers on the electric defects. The field enhancement factor that can be tolerated in the high field region of a cavity at this higher gradient is only 200. However, there is some evidence that the density of emission sites with $\beta_a \geq 200$ is not much different than the number already quoted for $\beta_a = 400$. If this proves true one can hope that extensive helium sputter processing or "surgical" removal of emission sites will consistently yield gradients of 14 MV/m.

END

DTIC

9-86